REPORT NO. 114

FEBRUARY, 1958

THE COLLEGE OF AERONAUTICS

CRANFIELD

An investigation into the flow over delta wings at low speeds with leading edge separation.

- by -

D.J. Marsden B.Sc., D.C.Ae., R.W.Simpson B.A.Sc., D.C.Ae.,

and W.J.Rainbird B.E., A.F R.Ae.S.

June, 1957.

SUMMARY

A low speed investigation of the flow over a 40° apex angle delta wing with sharp leading edges has been made in order to ascertain details of the flow in the viscous region near the leading edge of the suction surface of the wing. A physical picture of the flow was obtained from the surface flow and a smoke technique of flow visualization, combined with detailed measurements of total head, dynamic pressure, flow directions and vortex core positions in the flow above the wing.

Surface pressure distributions were also measured and integrated to give normal force coefficients.

The results of this investigation were compared with those of other experimental investigations and also with various theoretical results. In particular, the normal force coefficients, vortex core positions and attachment line positions were compared with the theoretical results of Mangler and Smith, reference 19. It was found that:

(i) Secondary vortices of opposite signs to the main vortices exist on the upper surface of the wing outboard of and below the main vortices. These secondary vortices are formed as a result of separation of the boundary layers developing outboard of the top surface attachment lines.

SUMMARY Continued.

(ii) The real flow was found to differ somewhat from the model of Mangler and Smith due to these secondary separations.

(iii) The "trailing edge" effect present at subsonic speeds was found to be considerable even at small angles of incidence. The normal force developed by spanwise strips exceeded that predicted by Mangler and Smith near the apex, but fell progressively as the trailing edge was approached. The centre of pressure is however approximately independent of incidence up to angles of incidence in excess of the semi apex angle.

1.

2.

3.

4.

5.

6.

TABLE OF CONTENTS

SYMBOLS

A		aspect ratio $= 4 \cot \Lambda = 4 K = (1.46$ for $\Lambda = 70^\circ)$
b		span (trailing edge)
C		local chord
c_r		root chord
$\bar{c}$		mean aerodynamic chord $= \frac{2}{3} c_r$ for delta wing. Its leading edge is $\frac{1}{3} c_r$ from the wing apex.
C_p	$= \frac{p - p_\infty}{\frac{1}{2} \rho U_\infty^2}$	pressure coefficient
ΔC_p	$= C_{p_L} - C_{p_U}$	
C_N	$= \int_{-s}^{+s} \frac{\Delta C_p}{2 s} dy$	local normal force coefficient per unit length
$\bar{C}_N$	$= \frac{N}{\frac{1}{2} \rho U_\infty^2 S} = \frac{2 \int_0^{c_r} C_N \, 2 s \, dx}{c_r b}$	overall normal force coefficient
H		Total head
h		height of vortex core above wing
K	$= \cot \Lambda = \tan \theta$	
p		static pressure
q_∞	$= \frac{1}{2} \rho U_\infty^2$	
s(x)		local semi-span
U_∞		freestream velocity
x, y, z		cartesian co-ordinates (x measured chordwise) (y measured spanwise)

α incidence

β secondary separation line angle to wing centre line

γ tertiary " " " " " " "

Λ leading edge sweepback

ρ density; attachment line angle to wing centre line

θ semi apex angle of delta

ϕ pitch angle

Appendix 1

a, b major and minor axes of ellipse

$h = b/a$

$s = \xi/a$ (fraction of semi span)

u_c = cross flow velocity component

ξ, η co-ordinates of ellipse

2. Introduction

The inviscid flow over slender flat wings, with the delta wing as a particular case, was treated by R.T.Jones (ref.9) in 1946. The real flow over slender wings with 'sharp' leading edges at incidence was found to differ from the Jones model in that separation of the boundary layers (developed outboard of the flow attachment lines on the pressure surface) occurred at the wing leading edges. The vortex sheets shed off these edges are blown back over the upper surface of the wing and roll up to form two stable vortex cores. These leading edge vortices, which are the main part of the trailing vortex system of the wing, considerably modify the flow field and result in non-linear lifting effects.

To account for this difference in the flow field, theories have been presented by Legendre (1953), Brown and Michael (1954), and Mangler and Smith (1957). All these theories represent the actual flow by theoretical models of increasing complexity. Legendre, reference 20, places isolated vortices above the wing such that the vortices are streamlines, and determines their strength by making the outflow tangential to the surface at the wing leading edges. Brown and Michael (ref.10) have included feeding vortex sheets along branch cuts from the leading edges to the vortices, and determined the position of the vortices from the condition that the overall force on the vortex and vortex sheet be zero. This model does not satisfy the boundary condition of zero pressure difference across the feeding vortex sheets. Mangler and Smith (ref.19) have assumed a curved shape for the vortex sheets feeding the vortex 'cores'. They have translated the exact three dimensional boundary conditions back into the cross flow plane, and solved the resulting problem by satisfying the condition that the pressure difference across the vortex sheets is zero at selected points on each sheet.

In all three of the above slender delta wing theories the flow has been assumed to be non-viscous and conical. The presence of a subsonic trailing edge, giving zero loading leads to the flow field being non-conical and this is not allowed for in the theories. The primary effect of viscosity, namely the leading edge separation, has been taken into account by allowing for the presence of the vortex sheets and rolled up vortex cores.

Örnberg (ref.2) and later Fink and Taylor (ref.1) showed by experiment that there are also 'secondary' viscous effects associated with the suction surface boundary layers. These boundary layers developing outboard of the top surface flow attachment lines eparate not at the sharp leading edges but somewhat inboard of these edges at spanwise positions slightly outboard of points under the main vortex cores where an adverse pressure gradient would be encountered. These 'secondary' spearations (so called by Maskell in ref.3) give rise to small triangular-shaped viscous regions on the suction surface near the leading edges.

This present report dicusses the results of a low speed flow investigation of this viscous region and its effect on the overall flow field.

3. Description of Apparatus.

3.1. Wind Tunnel.

The tests were performed in the College of Aeronautics 1B low speed wind tunnel at a velocity of 130 ft/sec.; lower speeds, about 80 ft/sec. were used for the surface flow and smoke visualization tests. The wind tunnel has an open working section, the jet size being elliptical, 40" wide x 27" high.

3.2. Models.

Model I was a sharp-edged (0.008" leading edge radius) delta wing with 60° leading edge sweepback. This model was only used for preliminary surface flow visualization tests.

Model II (see figure 1) was a sharp-edged (0.008") delta wing with 70° leading edge sweepback and a root chord of 18 in. The model was made from a 3/32" thick flat steel plate supported by a $\frac{3}{4}$" sting. Pressure plotting holes (0.018" dia) were drilled through the plate, on forty equiangular rays, into plastic tubing cemented to the plate under surface. Near the leading edge the section was too thin to accomodate the plastic tubing so slots were cut in the plate and araldite passages moulded into the edge. The under surface of the wing was filled with a metallic filler and painted black to provide good contrast for surface flow visualization tests. The wing thus has one flat surface and a blunt trailing edge see figure 1. The wing support sting was held in an incidence changing frame which pitched the model about a lateral axis through the centroid of area.

3.3. Traversing Gear and Pitch-Yaw Meter Tube.

The traversing gear was mounted on a base which could be tilted to the incidence of the model. It allowed translation along the full length of the model and across one half of the span. The traverse gear itself gave translation perpendicular to the surface and angular movement of 360° in yaw and $\pm 15^{\circ}$ in pitch. These angular movements were arranged so that the nose of the pitch-yaw probe remained in the same position.

Details of the yawmeter may be seen in Fig. 2. There are five tubes; a central tube for reading total head and four chamfered lateral tubes working in pairs to record pitch and yaw similar to a Conrad yawmeter.

By obtaining equal pressures from the yaw tubes and pitch tubes local flow direction could be found and total head was then read from the central tube. By rotating the head through 10° (in pitch, say), the dynamic head was also evaluated from the instrument calibration. The relatively large diameter (0.2") of the pitch-yaw meter prevented measurements being made very close to the wing surface. Also the length of the tube

prevented pitch angles towards the wing (say near the top surface attachment lines) from being measured close to the wing surface. The relatively large size of the tube is well illustrated in Figure 15 where its length is about half the local semi-span of the wing.

3.4. The Light Source and Smoke 'Bombs'.

The light source used was the same as the one used by Maltby and Peckham (Ref. 17). The cylindrical lenses were made up by turning thick perspex sheet on a lathe. It was necessary to supply cooling air to the lamp housing to prevent damage to the nearest perspex lens due to heating. The lamp used was an Osram type MA/V mercury vapour lamp of 400 watts giving 13600 lumens. It was overloaded 400% for six second periods to give a brighter light while photographs were being taken.

The smoke bombs were supplied by Brock's Crystal Palace Fireworks Ltd., Hemel Hempstead (Type W36E) and give a dense plume of white smoke for about 30 seconds. The smoke used was rather corrosive to unprotected steel surfaces.

4. Description of Tests.

4.1. Surface Flow Visualization.

Surface flow patterns at zero yaw for models I and II through an incidence range up to 30° are shown in figures 3, 4, 5, 6. These patterns were obtained using a mixture of 100 parts water, 40 parts alabastine powder and about 6 parts teepol by volume. The settled mixture is applied evenly to the model surface with a fine bristle paint brush. Small air bubbles on the surface leave fine traces in the surface powder as the air stream is turned on and the pattern dries. Low airspeeds (about 80 ft/sec.) were used since the pattern formed and dried quite rapidly under these conditions. Regions of intense surface shear stress, for example in the top surface boundary layer under the main vortex cores, dry very rapidly whereas near the secondary separation line where the excess surface liquid accumulates the pattern is probably distorted and dries slowly.

4.2. Surface Pressure meansurements.

Spanwise pressure distributions were obtained at four lengthwise stations for model II (see figure 1) using a conventional tilting multitube manometer. These are shown in Figs. 7, 8, 9 and 10 in non-dimensional form.

An incidence range up to 30° was covered in 2.5° steps at a speed of 130 ft/sec. Both pressure and suction surfaces readings were obtained by inverting the model. Corrections to incidence for rig deflection under load and wind tunnel interference have been applied; the latter are based on the formulae for small elliptically loaded wings with attached flow.

4.3. Flow Survey.

For model II a flow survey recording total head, dynamic pressure, and velocity direction was carried out at 3.9, 8.8, 14.0° incidence. The viscous region in a plane normal to the surface above station 2. (66.7% root chord) was investigated. The positions of vortex cores were traced for model II at 3.9, 8.8, 14.0°, incidence from the trailing edge to near the tip.

The survey of the flow above station 2 was carried out by taking readings at points on a grid of spanwise horizontal lines and lines perpendicular to the plane of the wing. Information obtained along these grid lines was plotted to give contours of constant total head and dynamic head. Some of these are seen in Fig.15.

Vortex core positions were determined by pointing the yawmeter towards the apex and translating vertically and horizontally to zero the yaw and pitch readings. This was thought to be fairly accurate since large yaw and pitch indications corresponded to small translational movements near the core.

The probe used was rather large and may influence the contours obtained but the readings were repeatable. The results are given in figures 16 to 19.

4.4. Smoke Flow Visualization Technique.

The flow over model II (70° Delta) was investigated using a smoke technique suggested by R.Maltby of the R A.E. Bedford. The flow in the cross flow plane is seen in figures 20 and 21 for station 2 along the chord and in the wake behind the trailing edge.

With the tunnel at a low speed, a smoke bomb was ignited in the settling chamber such that the plume of smoke went onto the apex of the model. A plane of parallel light from a mercury arc lamp and lens system was then passed across the model at the station under investigation and pictures taken looking down the model from the nose.

5. Discussion.

5.1. General Description of Flow.

The three dimensional model of the flow studied by Mangler and Smith is shown approximately in figure 22. The incident flow attaches to the wing surface along the lower surface attachment lines A_1. (The reader is referred to Maskell, reference 3, for a discussion of three dimensional flow separation and the definitions of flow separation and attachment lines.) These lines divide the surface flow passing over the trailing edge from that passing over the leading edge and are the three dimensional equivalent of the more familiar front stagnation streamline of two dimensional flow. The lower surface separation lines S_1 are along the sharp leading edges where a Kutta condition obtains. Two pseudo conical vortex sheets extend from the leading edges and roll up above the suction surface of the wing to form the vortex 'cores'. Due to the presence and strength of these vortices air is sucked down onto the top surface of the wing and two top surface attachment lines A_2 areformed. These attachment lines A_2 are considerably inboard of the lower surface attachment lines and with increase of incidence they move towards the centre line and coalesce. In Appendix I the predicted position of the lower surface attachment line for attached flow past elliptic cones is given; there is of course no upper surface attachment line in this case. Mangler and Smith have tabulated attachment line positions for their model of the flow - see Table III p.37 of reference 19, and have clarified the physical nature of these attachment lines by drawing radial projections of the three dimensional streamlines - see Figs. 15 and 16 of reference 19.

Air approaching the wing between the conical surface ab (see Fig.22) passes under the vortex core and flows out 'spanwise' whereas the air outside this region and between the top and between the bottom surface attachment lines flows in a more or less chordwise direction downstream and off the trailing edge.

The extra lift force produced by a delta wing with edge separations is then due to the extra entrainment of air by the vortices (see Weber reference 4). The non-linear nature of this extra lift is due to the inboard and upward displacement of the vortex cores and their increase of strength with increase of incidence, giving an ever increasing entrainment effect.

5.2. The Viscous Regions.

Figure 23 is a composite figure showing the total head survey, the upper surface pressure coefficient distribution, the surface flow and the smoke visualization results. These can be interpreted as indicating the type of viscous flow pattern shown in Fig.24 which has been sketched for an incidence of approximately 0.7 of the semi-apex angle ($\alpha = 14^{\circ}$). The boundary layer thicknesses shown are thicker than those actually present.

The thin (probably laminar) boundary layer developing outboard of the lower surface attachment lines A_1 separates at the edge and contributes most of the vorticity in the leading edge vortex sheet and main vortex core. The boundary layer inboard of A_1 on the lower surface would eventually leave the trailing edge. On the upper surface the boundary layer growing outboard of A_2 separates at the secondary separation line S_2 and rolls up to form a secondary core of 'opposite sign' to the main vortex. Figure 16 shows the pitch angles induced by this secondary core near the leading edge on the top surface. The presence of this secondary core was shown in the present experiments by a small ($\frac{1}{4}$" span) delta shaped vorticimeter which rotated in the opposite sense to the main vortex when placed at the core position of the secondary vortex. The component of the circulation at right angles to the cross flow plane was estimated for the circuits shown in figure 15. If the counterclockwise circulation around ABCEFGHD, embracing the main vortex core, is called 100 units then the circulation around HGFE embracing the secondary vortex core worked out to be - 18 units. On some of the surface flow pictures, for example figure 4 and 5, a third attachment line A_3 is evident quite close to the upper surface leading edge and inboard, quite close to S_2, is a third separation line S_3. This latter detail is more clearly evident in the surface flow pictures given by Drougge and Larson in reference 7. In the region R, see figure 24, where the air has lost much of its total head there is probably some turbulent mixing It is evident then that most of the upper surface boundary layer flow does not in fact enter the main vortex core, but contributes to the wake from the upper surface trailing edge and to the secondary vortex core. The existence of vorticity in the wake of opposite sign has been noted by previous experimenters and figure 21 shows a sequence of smoke pictures illustrating the rotation of the weak secondary core around the main vortex core after the flow has left the trailing edge.

The shape of the smoke pattern behind the trailing edge is very similar to the total head contours taken in a wake by Fink, reference 1. The main effect of the secondary separation seems to be to displace the main vortex core inboard and upwards which might be expected to give more lift than the Mangler and Smith theory as suggested in reference 4. It is interesting to note that separation at the leading edge only exists at all

angles of incidence, other than zero, when the leading edge is sharp. When the leading edge possesses curvature we can expect a very small range of incidence in which complete attachment of the flow occurs. At a larger incidence, but still relatively small in magnitude, the under surface boundary layer should separate close to the leading edge and reattach on the upper surface forming a separation bubble. This type of flow would be different from that discussed by Mangler and Smith since no rolling up of the vortex sheet from the wing undersurface takes place. However at still larger incidences we should expect the flow to degenerate into that described by Mangler and Smith except that the secondary separation would be present.

5.3. Comparison of Results with the theory of Mangler and Smith (references 11 and 19).

The surface pressure coefficient distributions are shown in figures 7 to 10. The shape of the upper surface pressure peaks at the forward station (station 4) is fairly flat with minor peaks corresponding to the positions of the main and secondary vortices. The shape and magnitude of the pressure distribution changes as the trailing edge is approached (see figure 11) and the flow field for low speed flow is clearly far from conical due to the "trailing edge effect". Figure 12 shows a comparison of the pressure coefficient distributions at the forward station with those predicted by Mangler and Smith. It is seen that the theoretical pressure peaks are much greater and narrower than the experimental results.

Spanwise integration of the pressure coefficient distributions gives the local normal force coefficient curves shown in figure 13 for the four stations. When a comparison is made with the curve given by Mangler and Smith for their A_4 boundary conditions, it is seen that the experimental results at the forward station lie above this curve. This is the result anticipated in section 5.1 (and reference 4) and is due to the presence of the secondary separation. The normal force coefficient curves for the other stations fall progressively below the theoretical curve due to the loss of loading as the subsonic trailing edge is approached.

One might anticipate on physical grounds that the presence of a subsonic trailing edge would have a small effect at small incidence and a progressively greater effect at larger incidence - this would give a forward shift of the overall centre of pressure. Figure 14, which shows the chordwise variation of C_N and Figure 14a which shows the normalised distributions of C_N along the root chord for various incidences (up to $\frac{\alpha}{K} \sim 1.5$) indicated that the centre of pressure shift from 0.57 c_r is small and the 'trailing edge effect' is rather independent of incidence. (This has been confirmed by independent balance measurements on delta wings with sharp leading edges).

The centre of pressure is at 0.57 C_r from the wing apex or 0.36 $\bar{C}$ behind the leading edge of the mean aerodynamic chord. Figure 14 shows the overall normal force coefficients are in agreement with the measurements made at R.A.E. on a range of delta wings.

The surface flow pictures, some of which are shown in figures 3, 4, 5 and 6, look misleadingly conical when it is remembered how much the pressure coefficients vary along rays through the apex. Measurements indicate however that none of the attachment or separation lines are in fact straight. In figure 25 the upper surface flow attachment line positions, measured close to the apex, are shown for Models I and II for various α/K. It is seen that these closely correspond which is a little surprising in view of the rather large 30° semi-apex angle of model I. Also included on the figure for comparison is the predicted position given by Mangler and Smith. The experimentally determined attachment line positions are see to lie a roughly constant amount inboard (for α/K between 0.2 and 1.0) due to the presence of the secondary separation region.

In fact this inward displacement is very nearly equal to the width of the secondary separation region (see figure 26). The upper surface secondary separation line positions are shown in figure 26 together with the tertiary separations (S_3) where these could be seen. The positions of these lines are undoubtedly distorted due to the accumulation of excess surface liquid when the patterns are being formed. Here the results for Models I and II do not coincide and the secondary separation region is relatively wider for the narrower wing.

The positions of the main vortex cores measured with the five tube pitch-yaw meter are given in figures 17 and 18. Figure 19 compares these results with the positions estimated from the flow field measurements and smoke pictures taken at $x/c_r = 0.667$, that is at station 2. Also included in the figure are some additional experimental points from Fink, reference 1, taken at $x/c_r = 0.417$ on a 10° semi-apex angle delta wing, and the theoretical estimates of Mangler and Smith, Legendre, and Brown and Michael. The path of the cores in the present case, with change of incidence is similar to Finks but a given position occurs at a different α/K. It should be remembered that in neither of these low speed experiments are the flow fields truly conical so that the agreement for the different lengthwise stations ($x/c_r = 0.667$ and $x/c_r = 0.417$) is largely fortuitous. For a given α/K the experimentally determined core positions are inboard and above the position given by the theory of Mangler and Smith due to the presence of the secondary separation. The experimental 'core', taken as the total head minimum, is however not exactly equivalent to the centre of the core region in

Mangler and Smith's model.

6. Conclusions.

(i) Vortices exist in the so called secondary separation regions on the upper surface of a delta wing with sharp leading edges. Fluid rotation in the secondary cores is in the opposite sense to that of the main leading edge vortices. The secondary vortices contribute to the vorticity of opposite sign found in the wake system of these wings.

(ii) The secondary separation regions are fairly extensive on flat narrow delta wings and cause an inboard and upward displacement of the vortex cores compared to the positions given by Mangler and Smith in reference 19.

(iii) In low speed flow the forward positions of a delta wing will give more lift than predicted in reference 19 due to the secondary separations. The shape of local spanwise loading determined experimentally has much flatter peaks under the vortices than the theoretical distribution.

(iv) With a subsonic trailing edge there is of course a marked loss of loading towards this edge but the effect is not highly independent on incidence and the centre of pressure remains fixed for incidences up to 1.5 times the semi apex angle.

REFERENCES

1.	Fink, P.T. and Taylor, J.	Some low speed experiments with 20° Delta wings. A.R.C.17854.(1955).
2.	Ürnberg, T.	A note on the flow around delta wings. K.T.H. T.N.38 (1954).
3.	Maskell, E.C.	Flow separation in three dimensions. R.A.E.Aero 2565.(1955).
4.	Weber, J.	Some effects of flow separation on slender delta wings. R.A.E. T.N.2425.(1955).
5.	Lee, G.H.	Note on the flow around delta wings with sharp leading edges. Handley Page Interim Report S.W.A.C. Paper, No. S.0149 (1955).
6.	Fink, P.T.	Some low speed aerodynamic properties of cones. A.R.C.17632 (1955).
7.	Drougge, G. and Larson, P.O.	Pressure measurements and flow investigation on delta wings at supersonic speed. F.F.A.Report 57.(1956).
8.	Pocock, P.J. and Laundry, W E.	Some aerodynamic characteristics of delta wings at low speeds. Second Canadian Symposium on Aerodynamics Institute of Aerophysics, Univ. of Toronto, (1954).
9.	Jones, R.T.	Properties of low aspect ratio pointed wings at speeds above and below the speed of sound. N.A.C.A.Report 835,(1946).
10.	Brown, C.E. and Michael, W.H.	Effect of leading edge separation on the lift of a delta wing. J.Ae.Sc. Vol.21 (1954).
11.	Mangler, K.W. and Smith, J.H.B.	A theory of slender delta wings with leading edge separation. R.A.E. T.N.Aero 2442. (1956).

12.	Brebner, G.G.	Boundary layer measurements on a 59° swept back wing at low speeds. A.R.C. C.P.86 (1952).
13.	Stalker, R.J.	A study of the china film technique for flow indication. A.R.L. Report A96.
14.	Bartlett, G.E. and Vidal, R.J.	Experimental investigation of influence of edge shape on the aerodynamic characteristics of low aspect ratio wings at low speeds. N.A.C.A. T.N.1468 (1947).
15.	Orlik-Rückemann, K.	Experimental determination of pressure distributions and transition lines of plane delta wings at low speeds and zero yaw. Swedish K.T.H. Aero Tech. Note 3 (1948).
16.	Küchemann, D.	Types of flow on swept wings with special reference to free boundaries and vortex sheets. J.R.Ae.Soc. Nov.1953.
17.	Maltby, R.L. and Peckham, D.H.	Low speed flow studies of the vortex patterns above inclined slender bodies using a new smoke technique. R.A.E. T.N.Aero 2482 (1956).
18.	Prandtl, L.	The essentials of fluid dynamics. Blackie and Sons (1952).
19.	Mangler, K.W. and Smith, J.H.B.	Calculation of the flow past slender delta wings with leading edge separation. R.A.E. Aero 2593 (1957).
20.	Legendre, R.	Ecoulement au voisinage de la pointe avant d'une aile à forte flèche aux incidences moyennes. La Recherche Aeronautique (O.N.E.R.A.) No. 31 1953.

APPENDIX I

Attachment lines on a family of elliptic cones.

Consider a family of slender bodies of elliptical cross-section. Let us assume the flow can be resolved into an axial and a cross flow. If U_∞ is the freestream velocity and the body is at a small incidence α we can assume, since the body is slender that the perturbation axial velocity component is small compared with $U_\infty \cos \alpha$. The resultant of the axial velocity component, $U_\infty \cos \alpha$ and the cross-flow velocity component u_c gives the surface flow direction (in inviscid flow). Under certain conditions of body shape and incidence the resultant velocity vector will lie on a generator passing through the body apex. This line will be called either an attachment line or a separation line depending on whether the flow near the generator is respectively away from or towards the generator.

If the ellipse has major and minor axes of lengths a and b respectively the circumferential cross-flow velocity on the surface of the ellipse at (ξ, η) due to the cross-flow component of the freestream velocity, $U_\infty \sin \alpha$,

$$\text{is} \quad u_c = \frac{2 U_\infty \sin \alpha \, \xi/a}{\sqrt{(1 - \frac{a-b}{a+b})^2 + 4(\frac{a-b}{a+b}) \, \eta^2/b^2}} \qquad (1)$$

If $b/a = h$ (a height factor describing the thickness of the ellipses)

$= 0$ for a flat plate

$= 1$ for a circle.

$\tan \theta = K = a/c_r$ where θ is the semi-apex angle (spanwise) and c_r is the root chord

$$\text{then} \quad u_c = \frac{U_\infty \sin \alpha \, s(1 + h)}{\sqrt{1 - s^2 (1 - h^2)}} \qquad (2)$$

where $s = \xi/a$ (fraction of semi span)

It can be shown that the resultant flow is along a generator if

$$\frac{u_c}{U_\infty \cos \alpha} \qquad \frac{Ks\,(1 - S^2)(1 - h^2)}{\sqrt{1 - S^2\,(1 - h^2)}} \tag{3}$$

Thus equating (2) and (3) the flow is along a generator if

$$s = \pm \sqrt{1 - \left(\frac{\alpha}{K(1-h)}\right)^2} \tag{4}$$

when $h = 0$ (flat plate) $s = \pm \sqrt{1 - \left(\frac{\alpha}{K}\right)^2}$ (5)

$h = 1$ (circle) s is imaginary unless $\frac{\alpha}{K} = 0$

In all cases for real s $\frac{\alpha}{K} \leqslant (1-h)$

For a narrow delta wing with attached flow at the leading edge the undersurface attachment line id described by (see (5))

$$s = \pm \sqrt{1 - \left(\frac{\alpha}{K}\right)^2}$$

For values of α/K less than one there are two attachment lines on the undersurface which reduce to one when $\alpha/K = 1$. When the flow is separated at the leading edge the undersurface flow is not changed appreciably. Hence the undersurface attachment lines are still given approximately by (5).

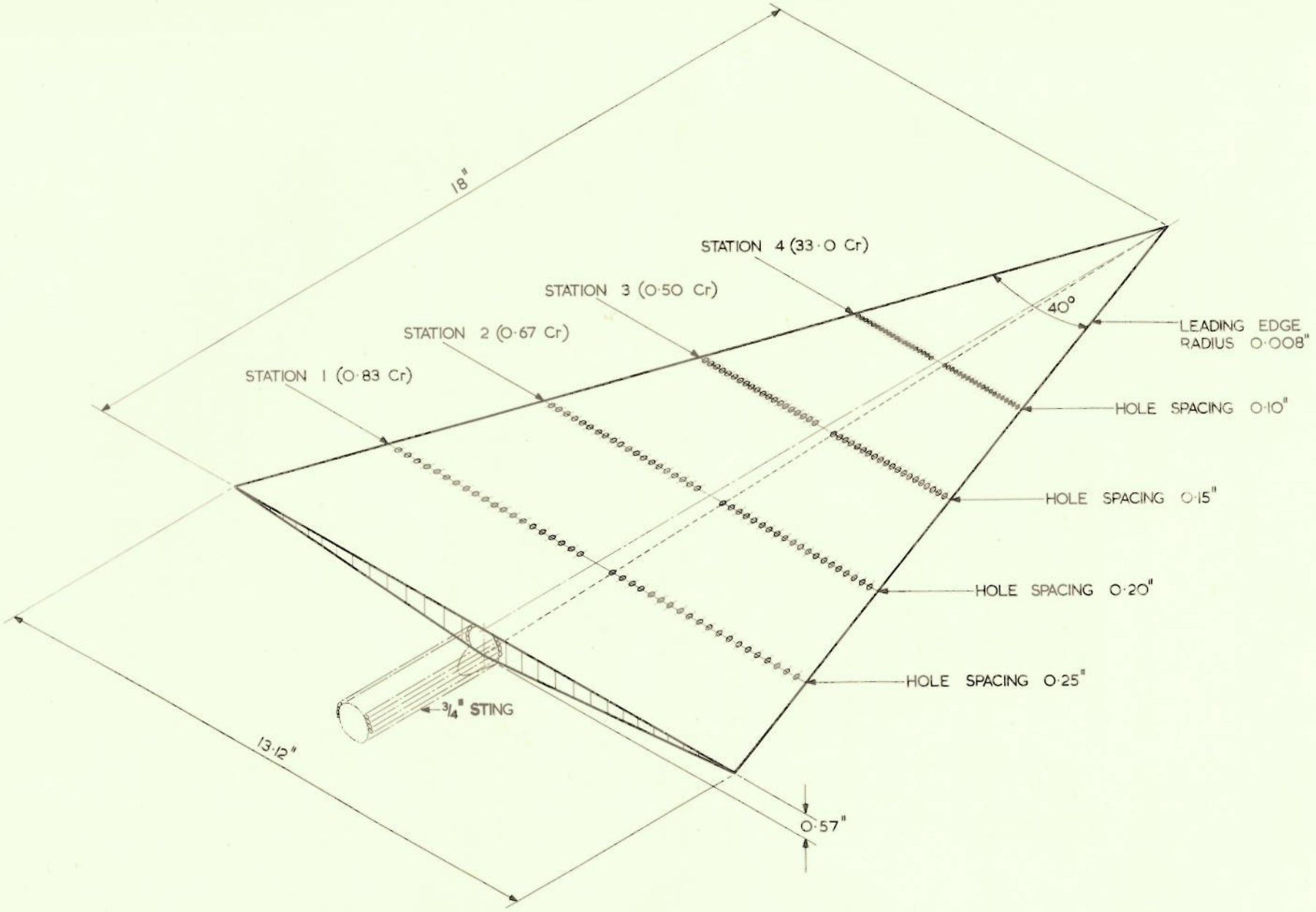
18"
STATION 4 (33·0 Cr)
STATION 3 (0·50 Cr)
STATION 2 (0·67 Cr)
STATION 1 (0·83 Cr)
40°
LEADING EDGE
RADIUS 0·008"
HOLE SPACING 0·10"
HOLE SPACING 0·15"
HOLE SPACING 0·20"
HOLE SPACING 0·25"
3/4" STING
13·12"
0·57"

FIG. 1.

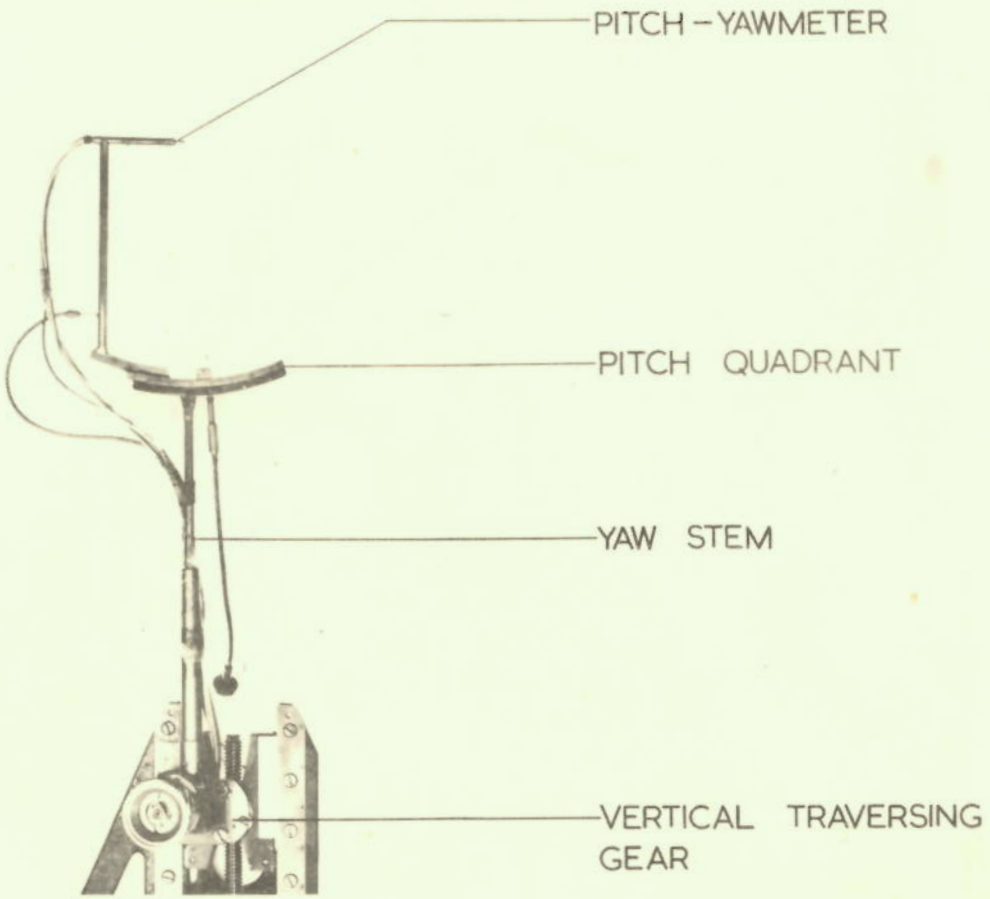

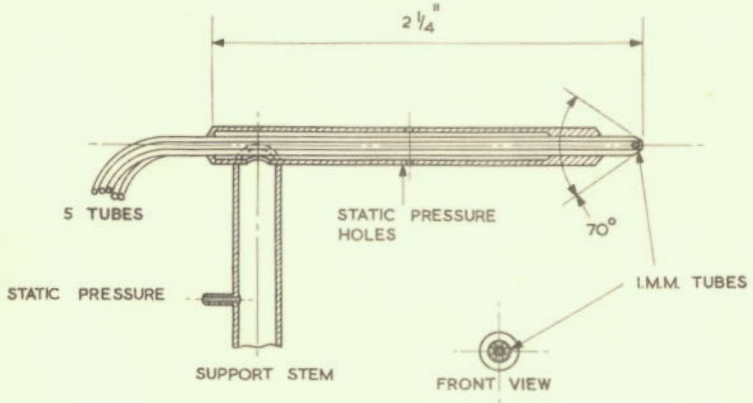

YAWMETER HEAD DETAILS

SCALE 2 : 1

FIG. 2.

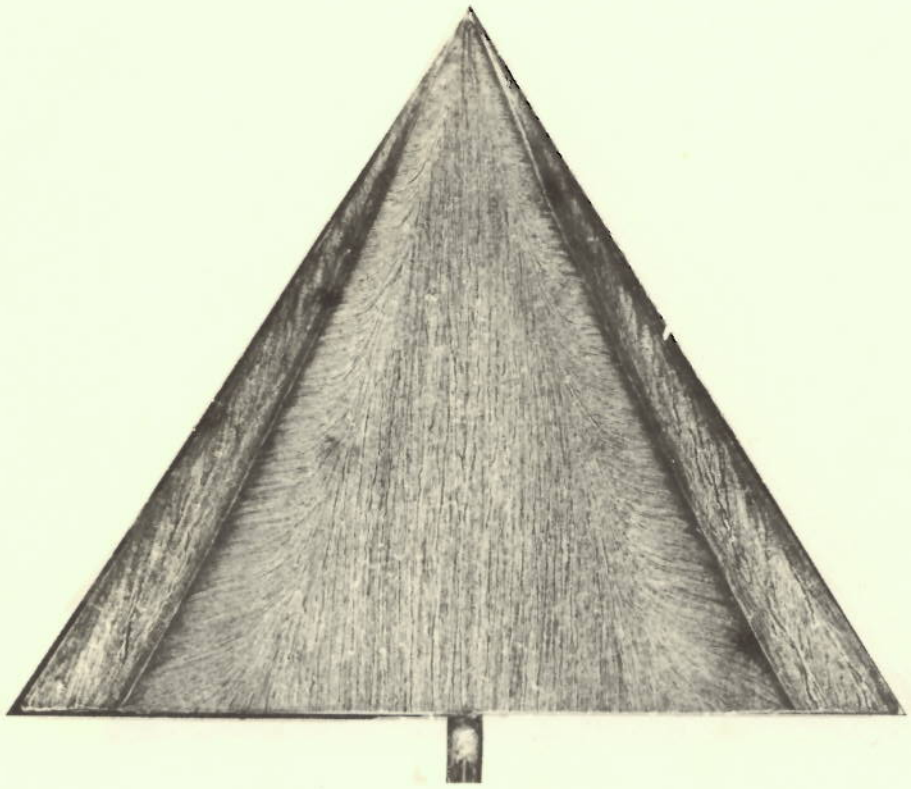

FIG. 3. SURFACE FLOW VISUALISATION ON UPPER SURFACE - MODEL I ($\Lambda = 60^{\circ}$) $\alpha = 14^{\circ}$

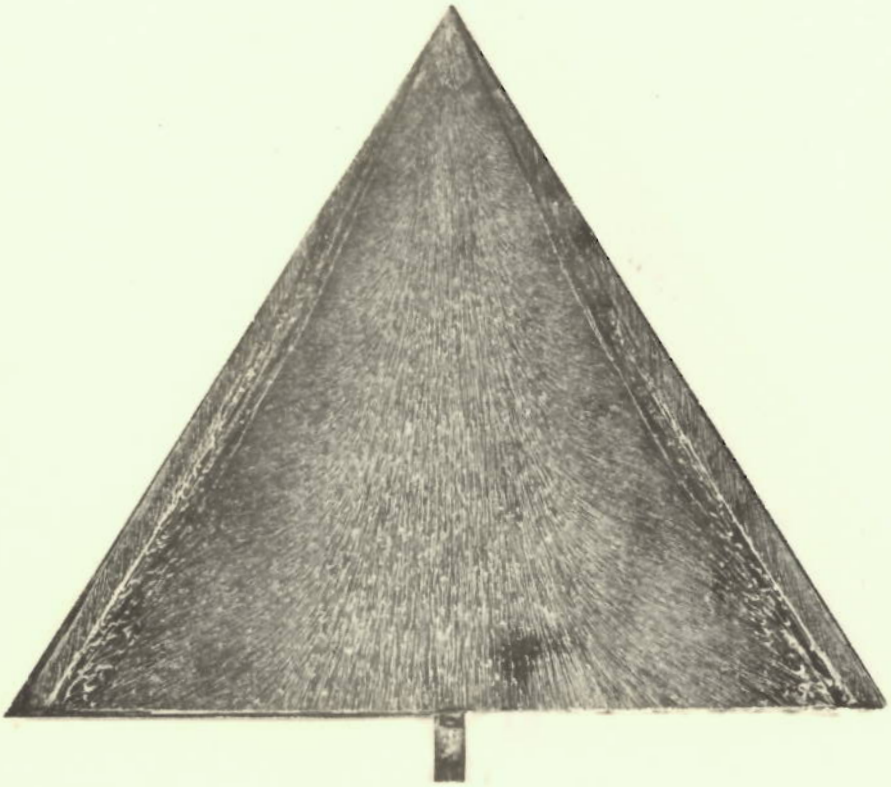

FIG. 4. SURFACE FLOW VISUALISATION ON UPPER SURFACE - MODEL I ($\Lambda = 60^{\circ}$) $\alpha = 23.9^{\circ}$

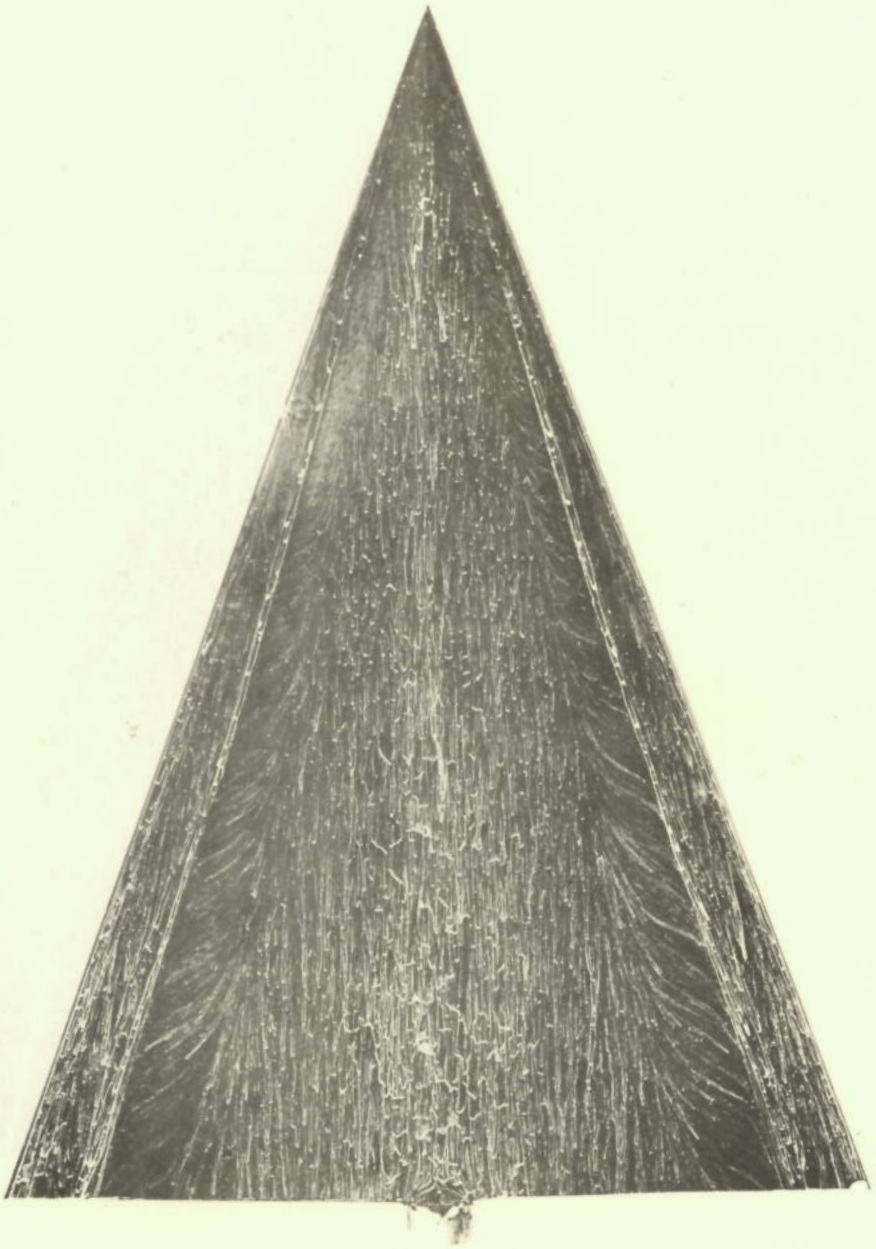

FIG. 5. SURFACE FLOW VISUALISATION ON UPPER SURFACE - MODEL II ($\Lambda = 70^{\circ}$) $\alpha = 6.3^{\circ}$

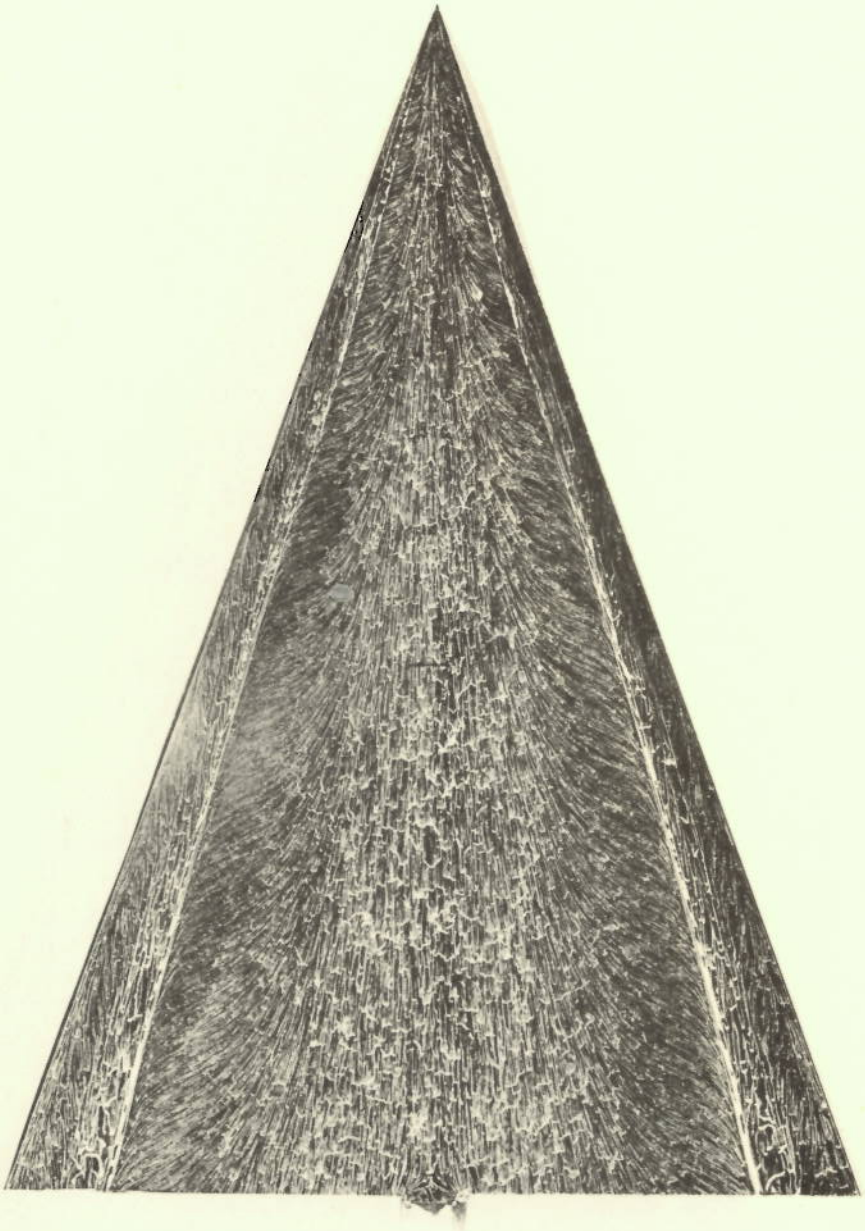

FIG. 6. SURFACE FLOW VISUALISATION ON UPPER SURFACE - MODEL II ($\Lambda = 70^{\circ}$) $\alpha = 14.0^{\circ}$

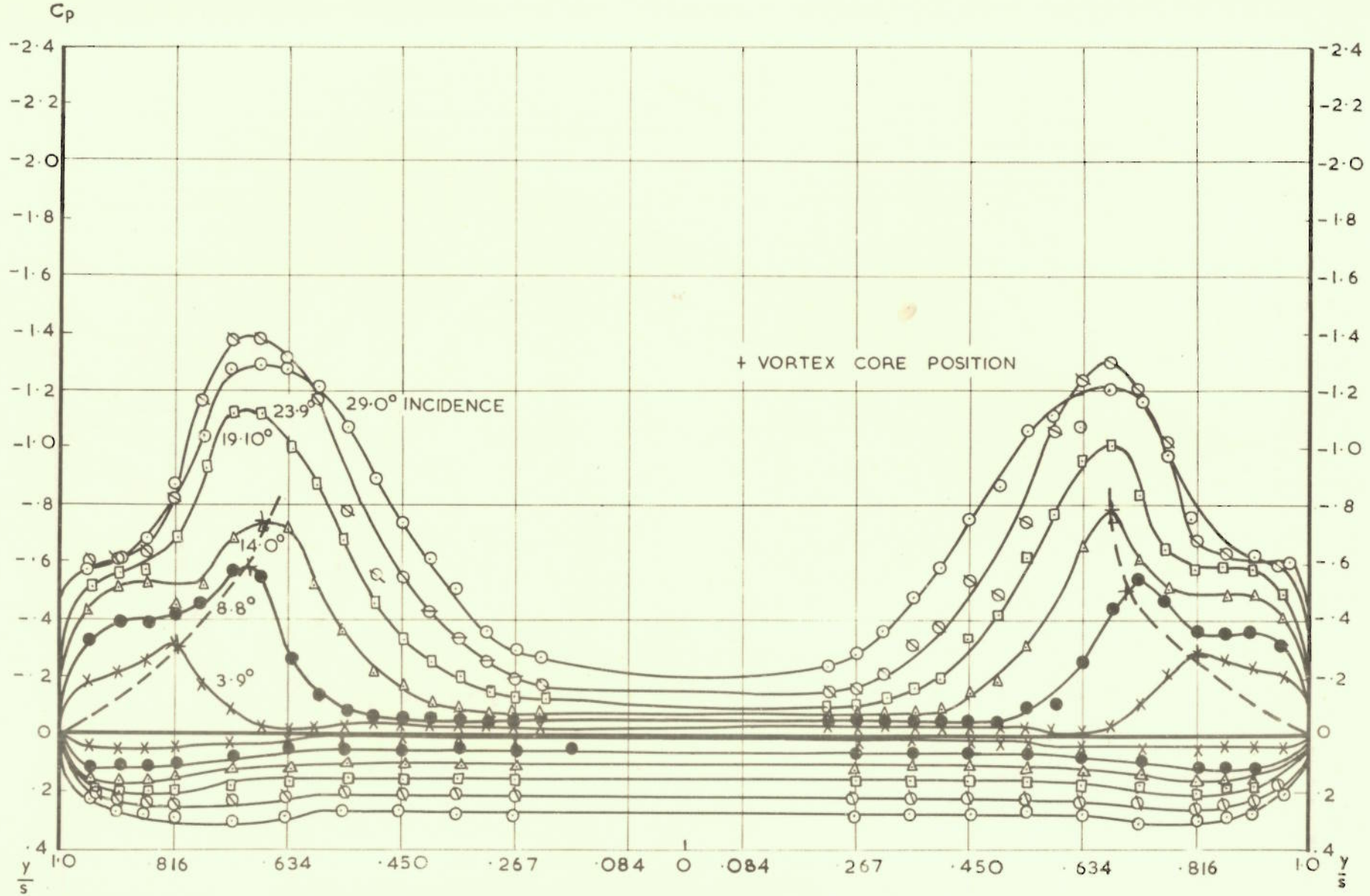

FIG. 7 SPANWISE VARIATION OF Cp STATION 1 MODEL II

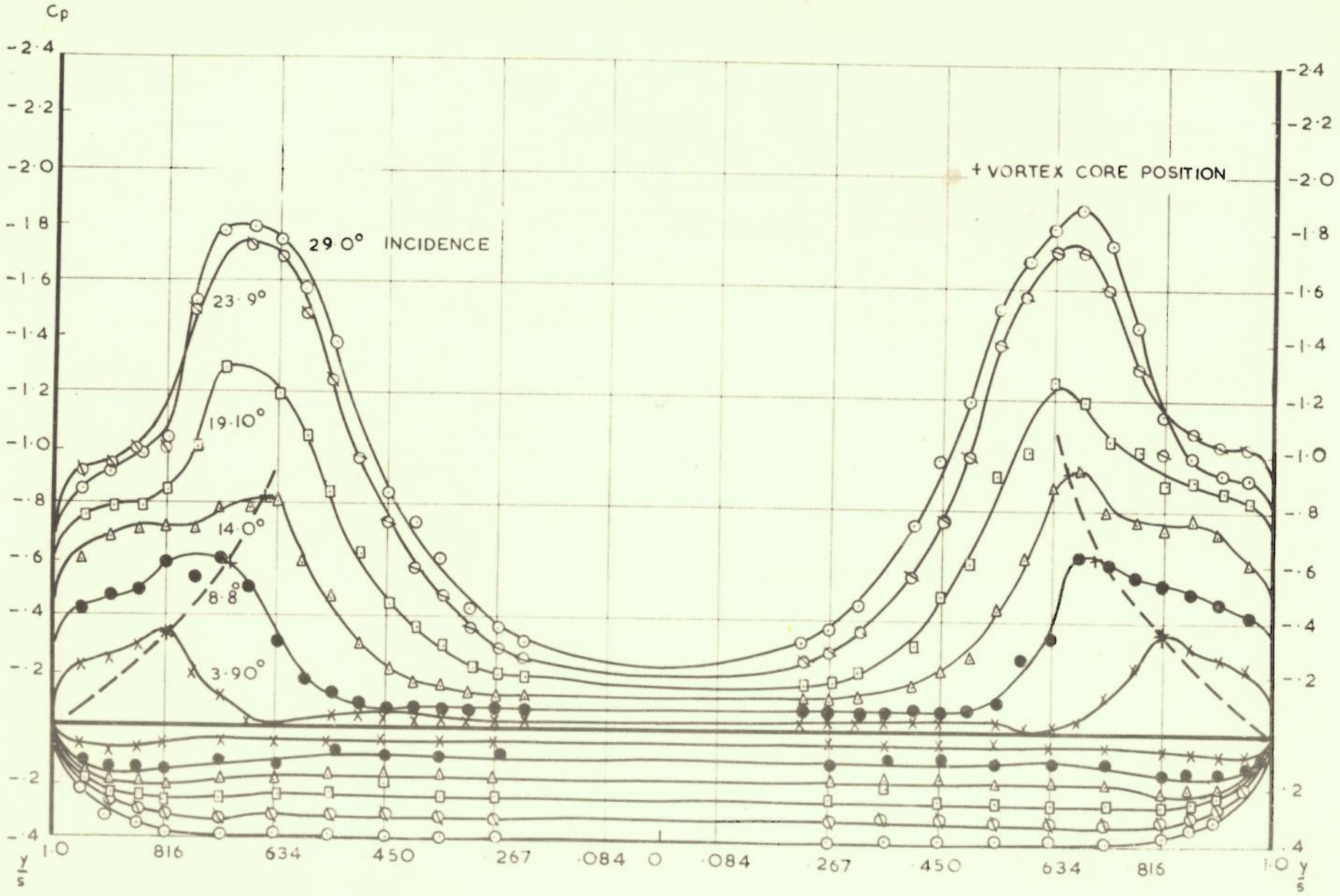

FIG. 8 SPANWISE VARIATION OF C_p STATION 2. MODEL II

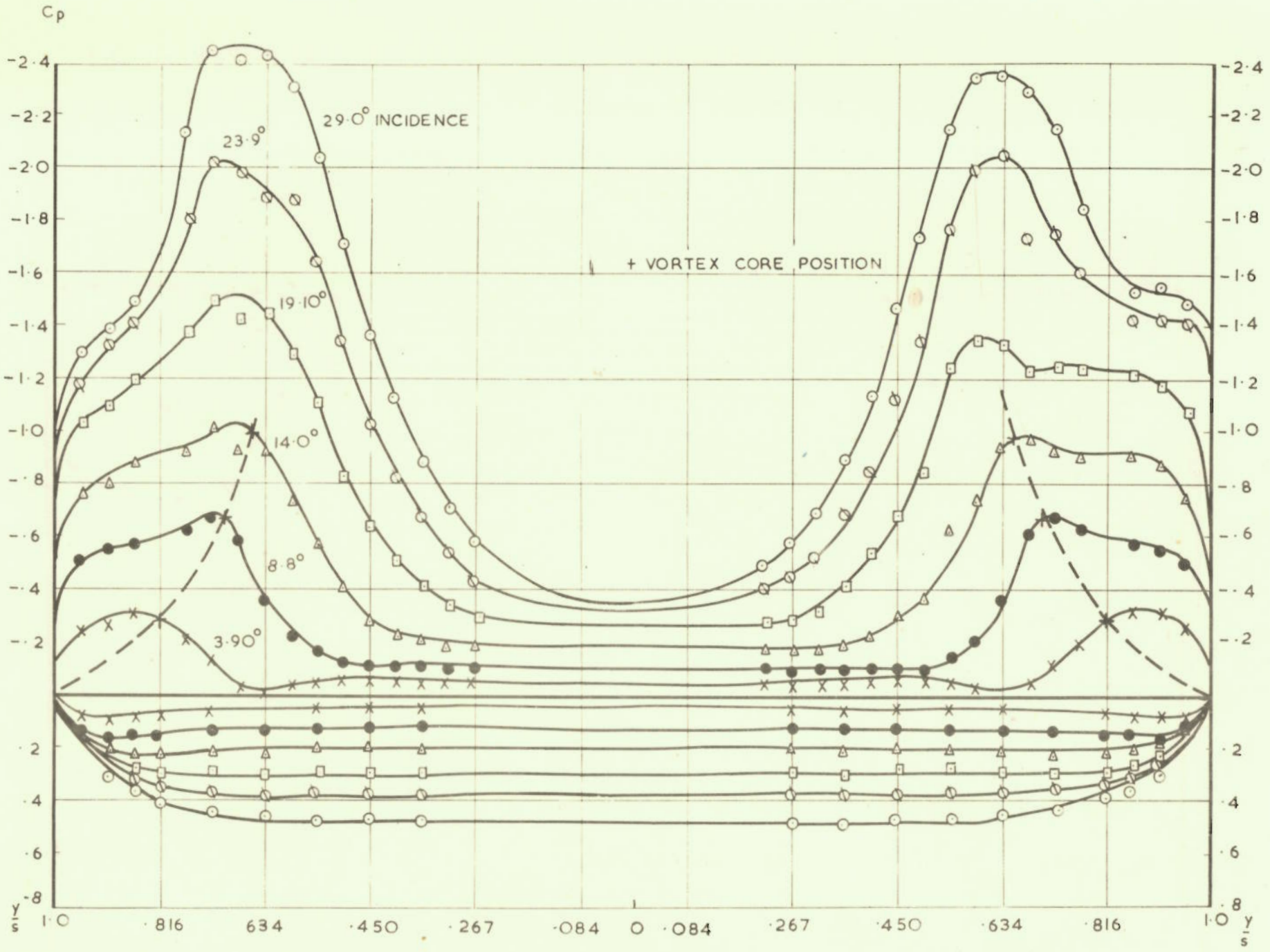

FIG. 9 SPANWISE VARIATION OF Cp STATION 3 MODEL II

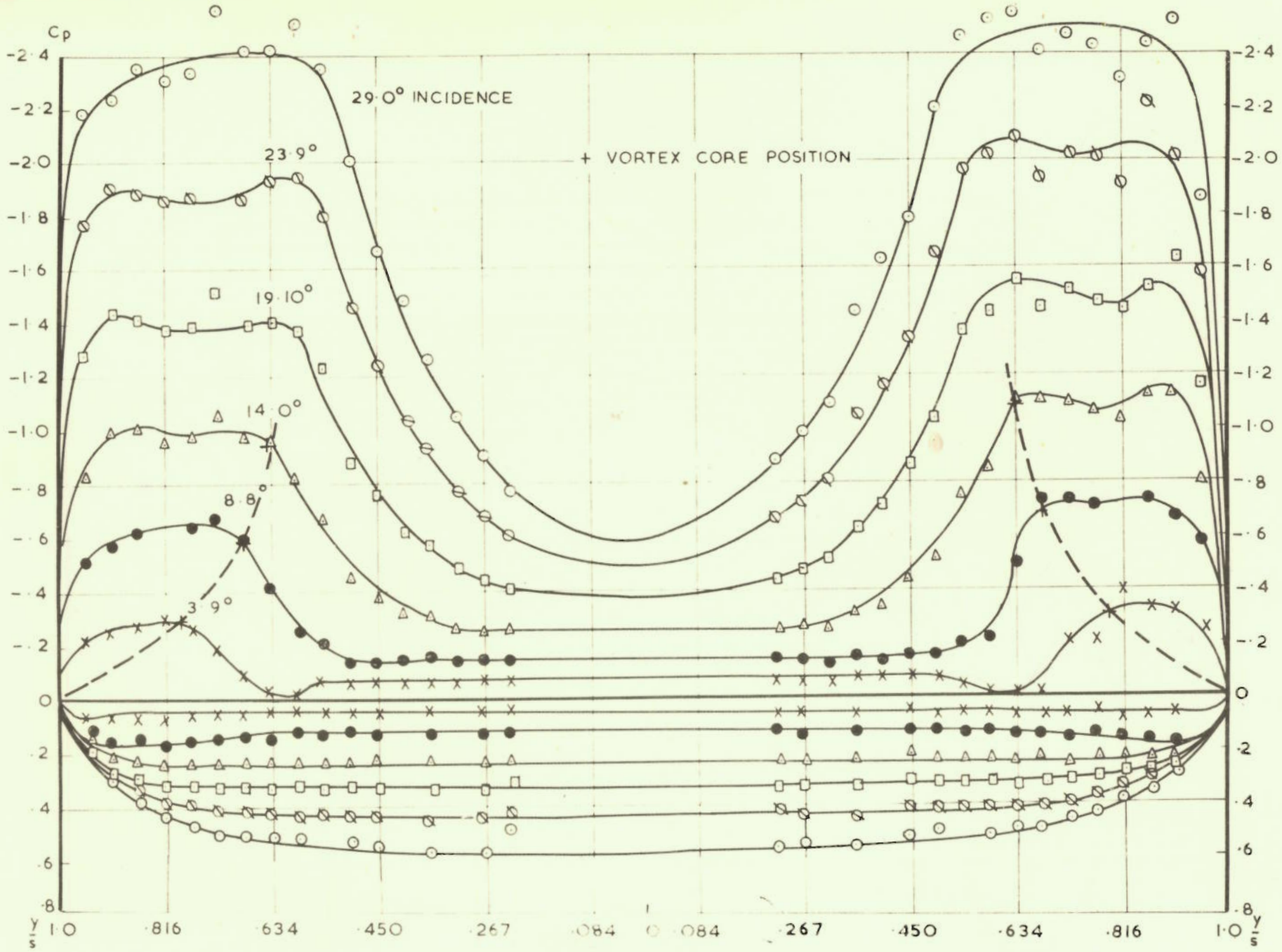

FIG. 10 SPANWISE VARIATION OF Cp. STATION 4 MODEL II

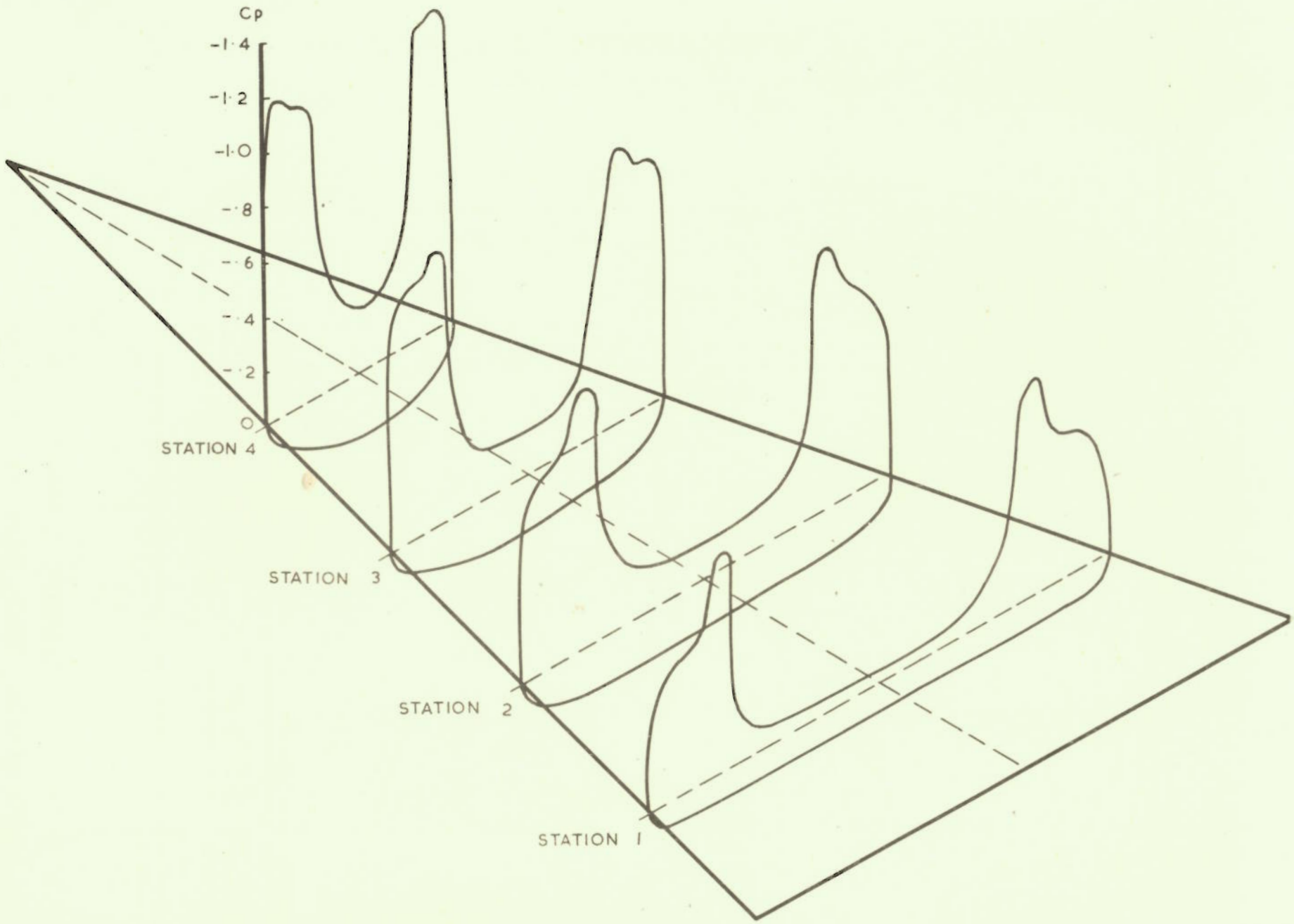

FIG. 11 PRESSURE DISTRIBUTION AT 14·0° INCIDENCE (Λ = 70°)

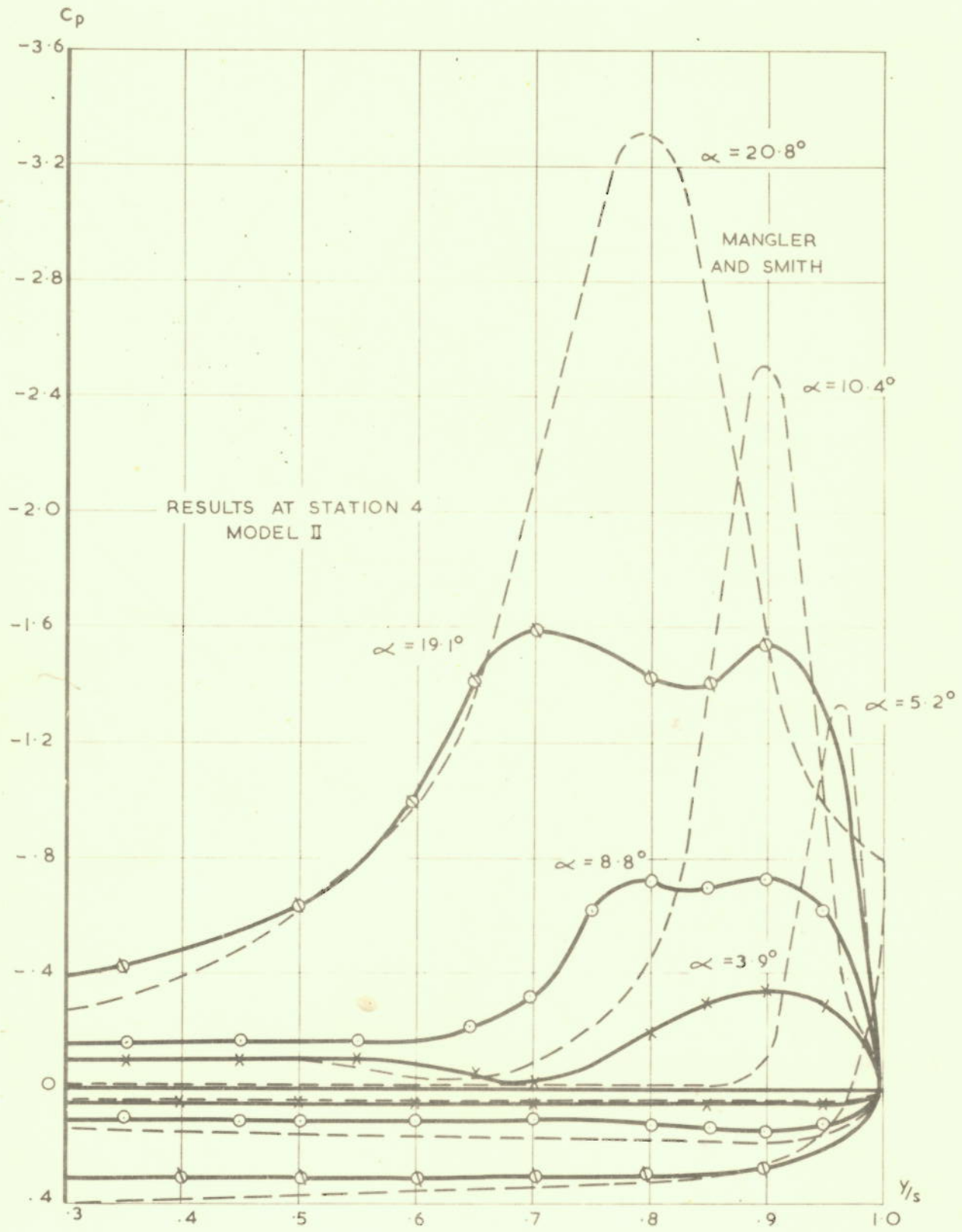

FIG. 12 SPANWISE PRESSURE DISTRIBUTIONS
(COMPARISON WITH RESULTS OF MANGLER AND SMITH)

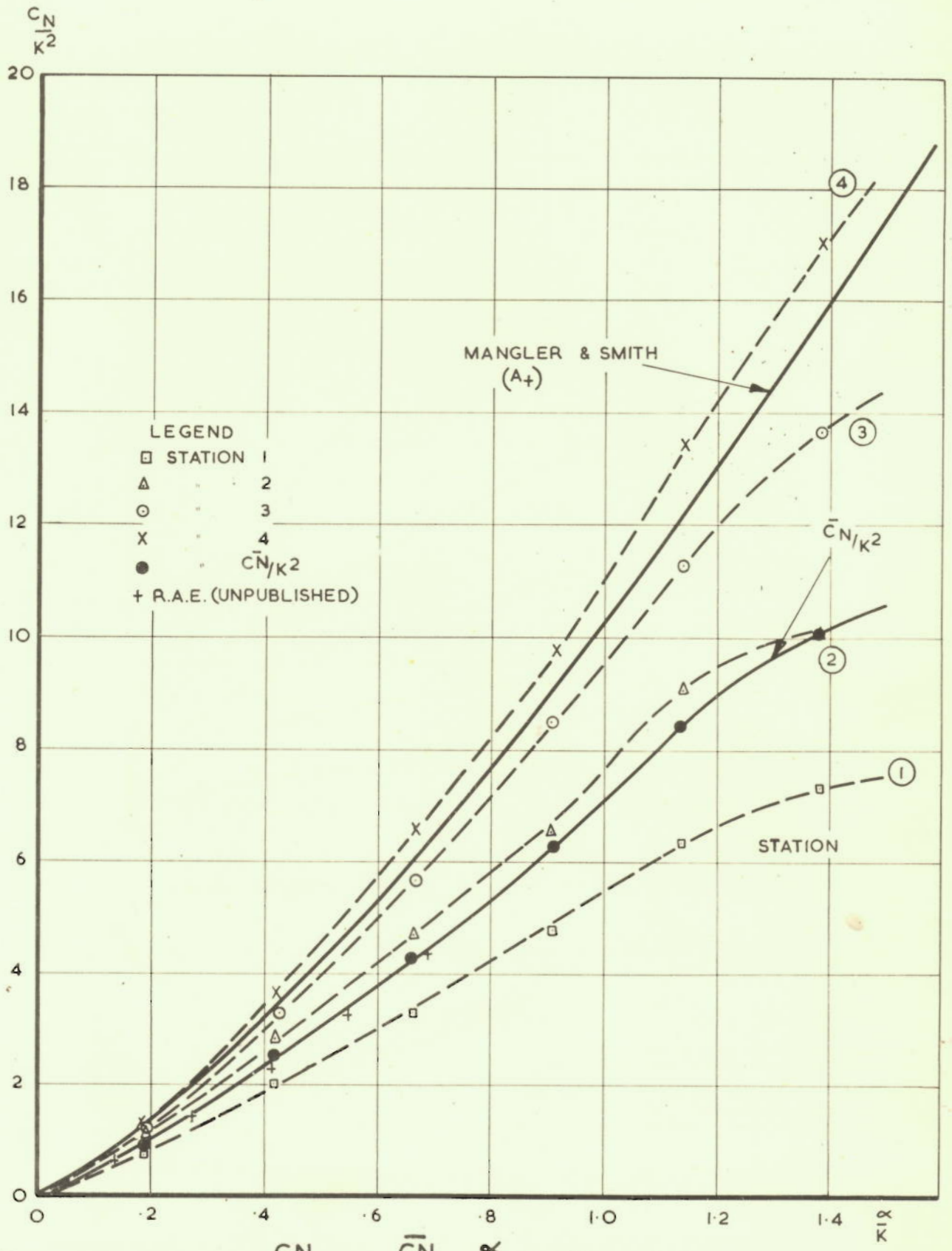

FIG. 13 VARIATION OF $\frac{CN}{K^2}$ AND $\frac{\bar{C}N}{K^2} - \frac{\alpha}{K}$ FROM PRESSURE DISTRIBUTIONS AT STATIONS 1, 2, 3, 4, MODEL II.

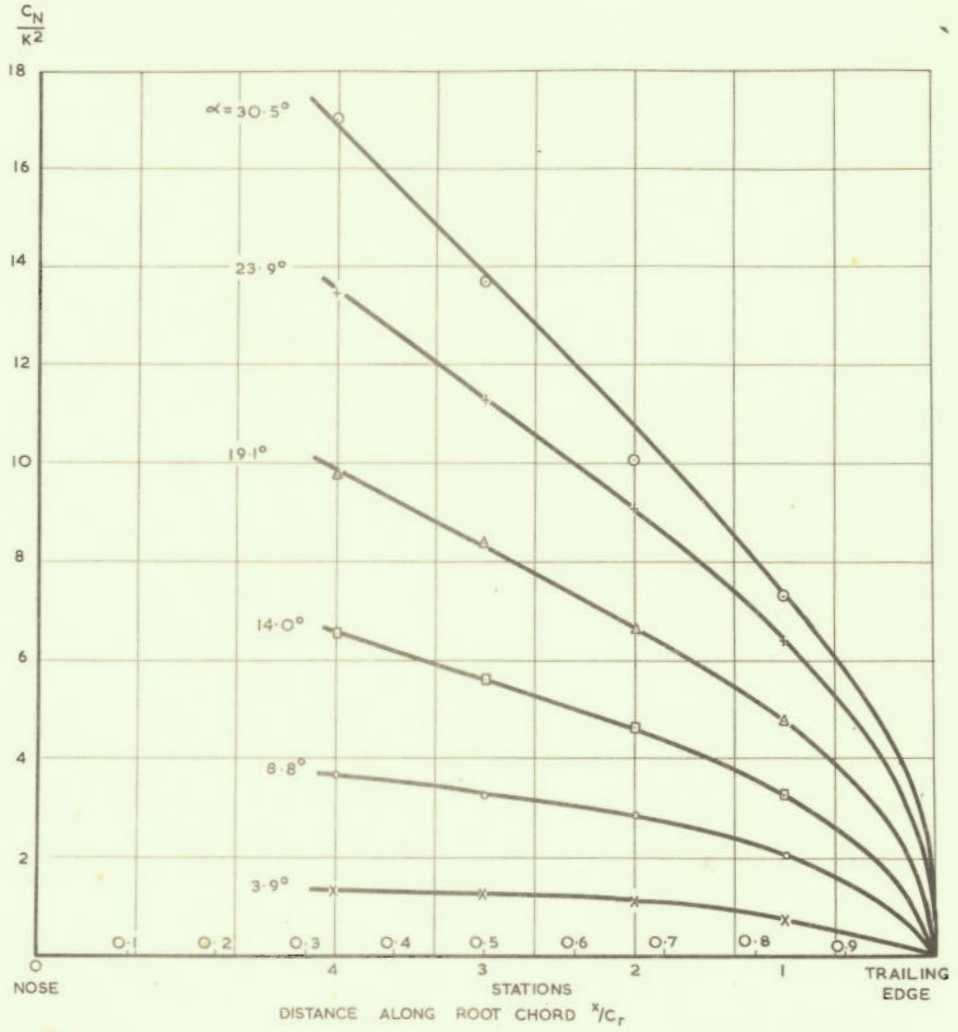

FIG. 14 A. CHORDWISE VARIATION OF $\frac{C_N}{K^2}$ WITH INCIDENCE. MODEL II

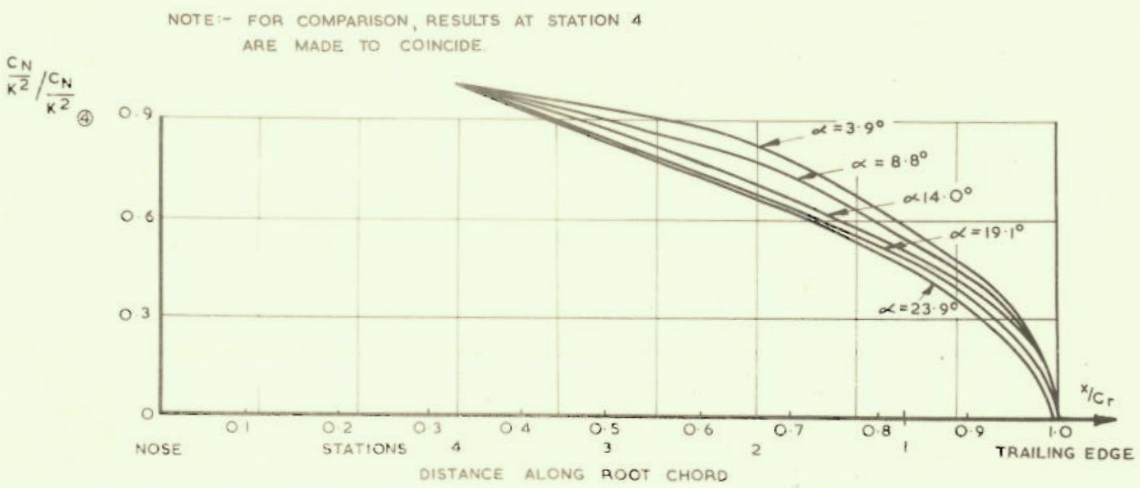

FIG. 14 B VARIATION OF SHAPE OF C_N DISTRIBUTION WITH INCIDENCE MODEL II

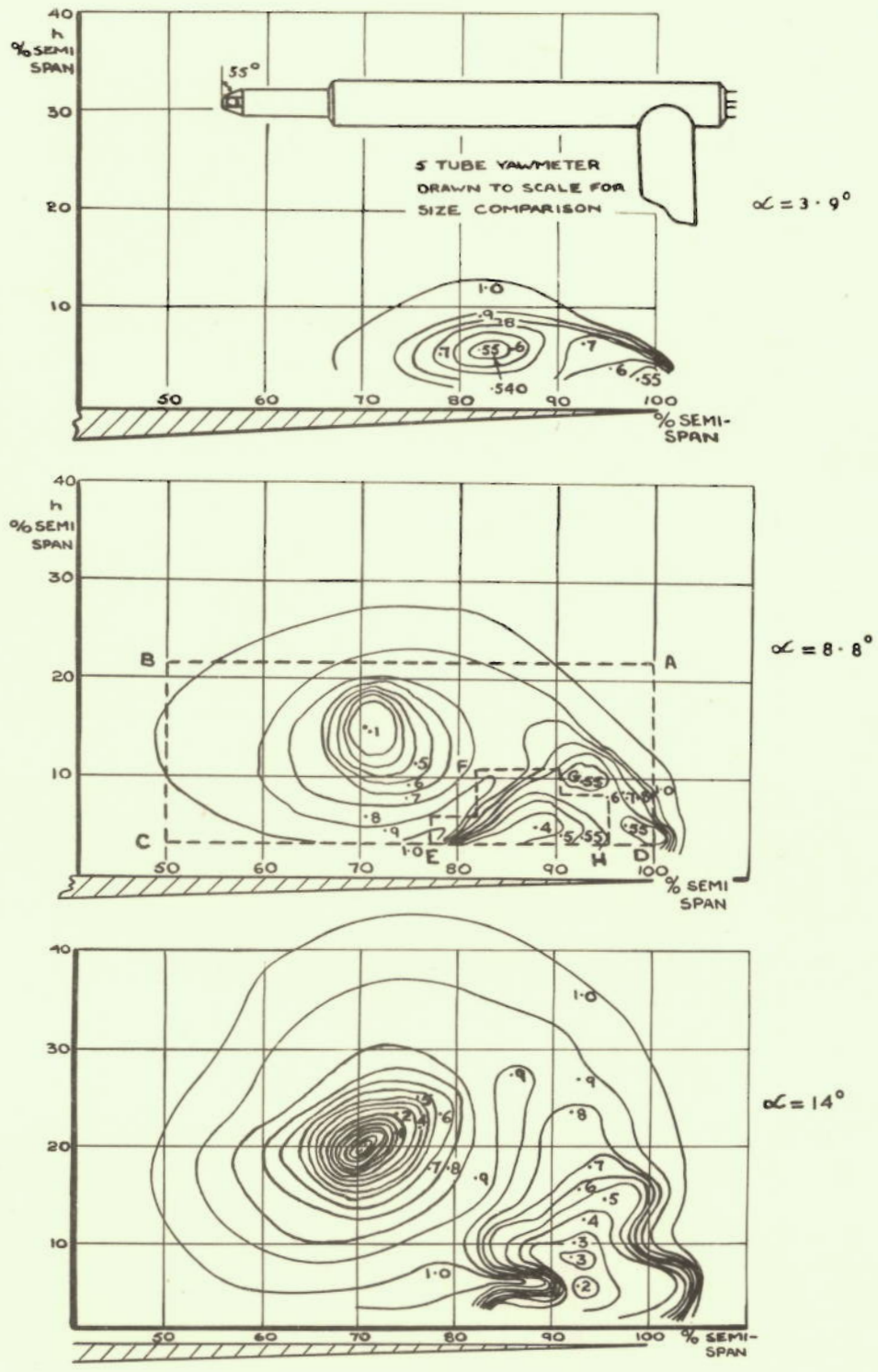

FIG. 15. TOTAL HEAD SURVEY AT STATION 2 $(0{\cdot}67c_r)$
AT $\alpha = 3{\cdot}9°$ $8{\cdot}8°$ AND $14°$
(LINES OF $\frac{H-p_\infty}{q_\infty}$ = CONSTANT)

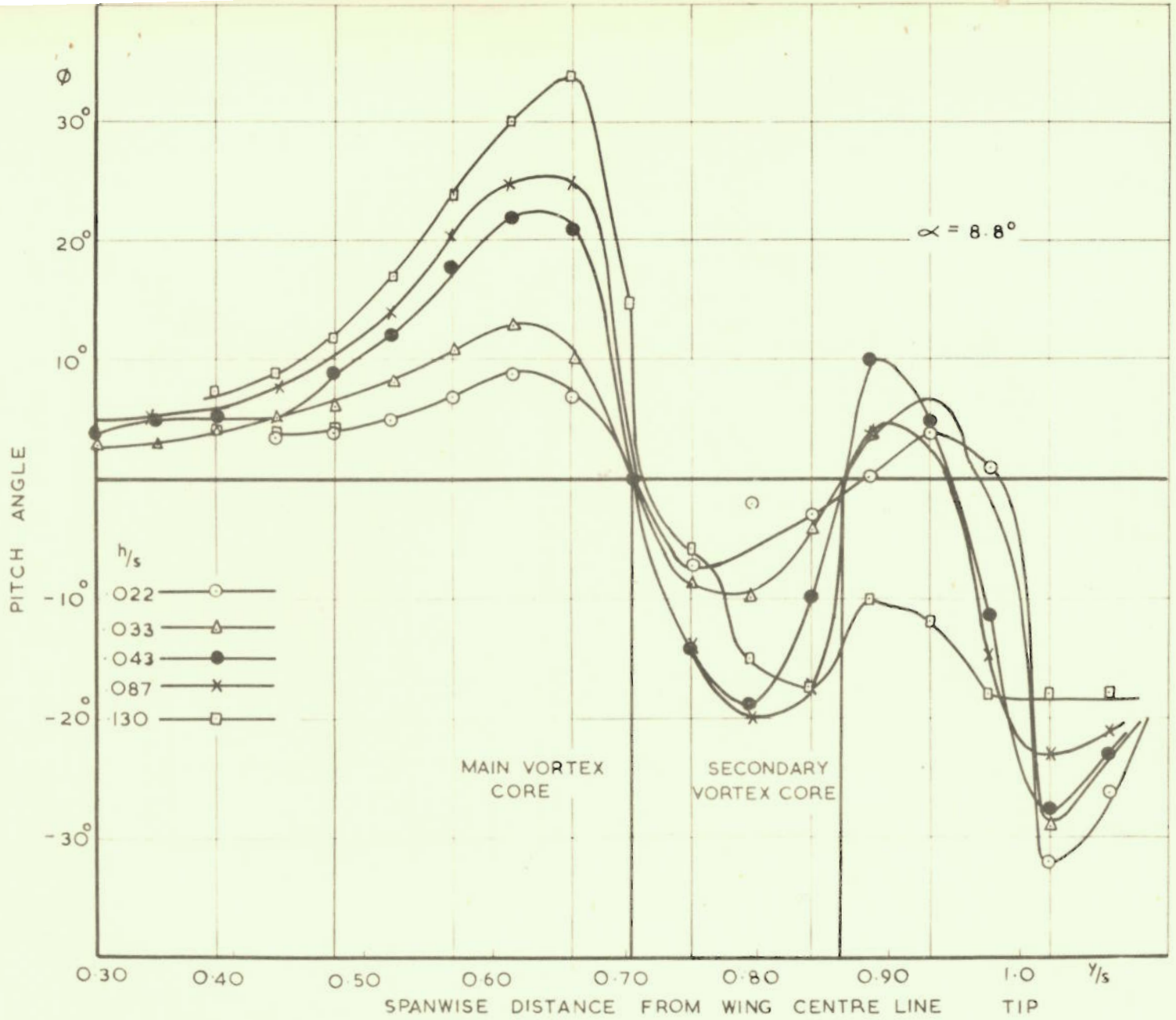

FIG. 16 SPANWISE VARIATION OF PITCH ANGLE. TOWARDS WING SURFACE

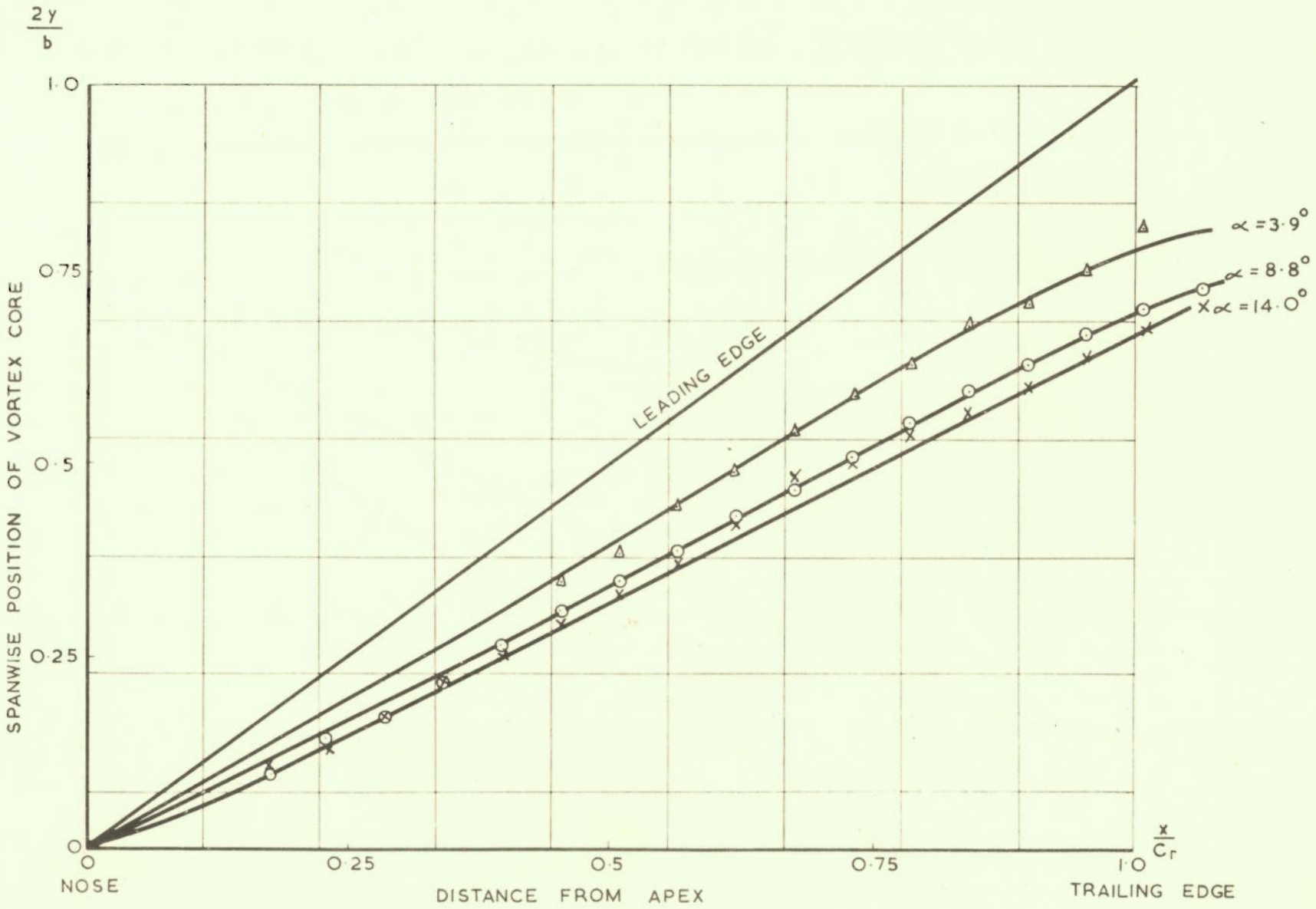

FIG. 17 SPANWISE POSITION OF VORTEX CORE MEASURED WITH YAWMETER MODEL II ($\Lambda = 70°$)

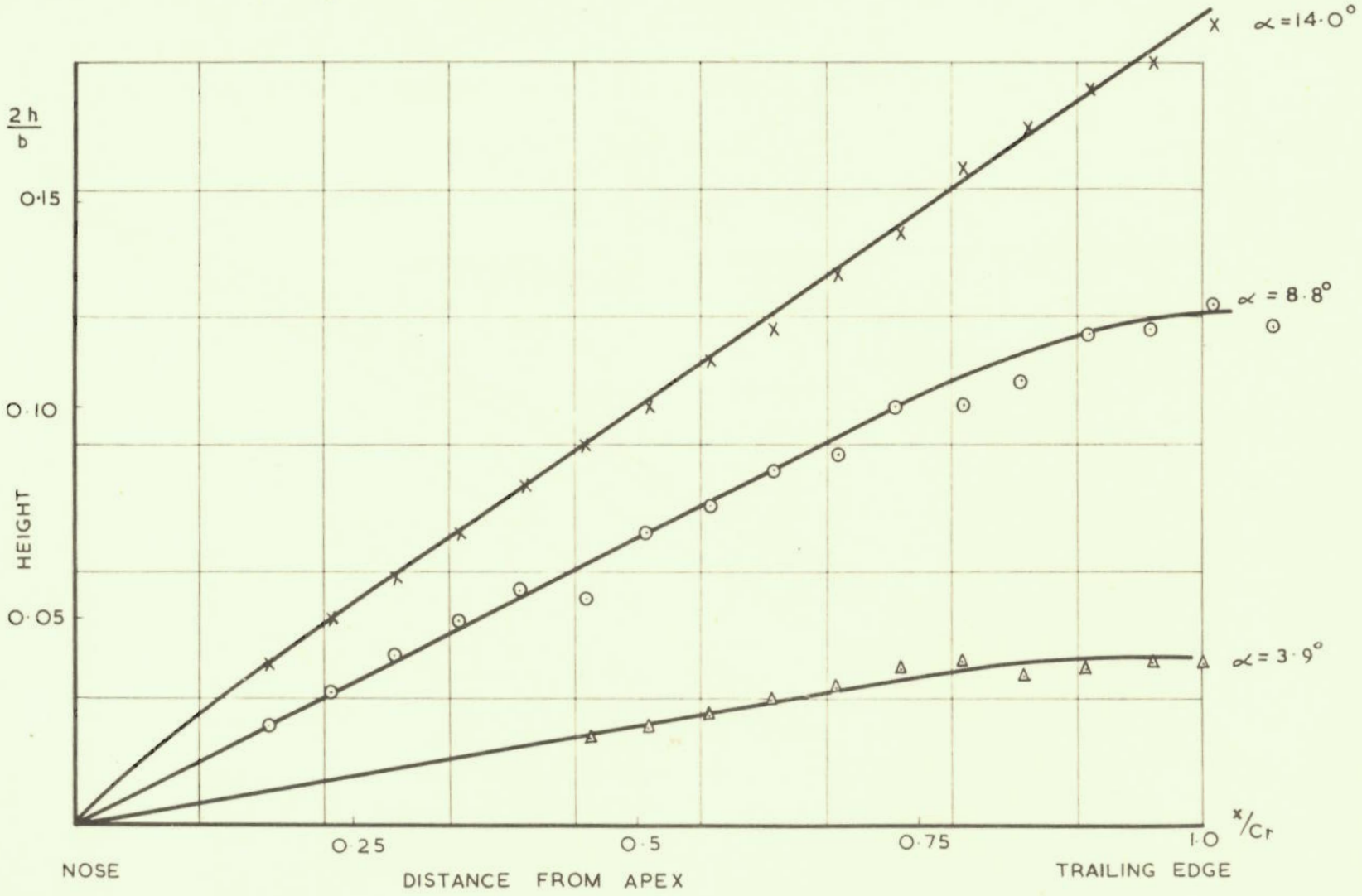

FIG. 18 CHORDWISE VARIATION OF VORTEX HEIGHT MODEL II ($\Lambda = 70°$) MEASURED WITH YAWMETER.

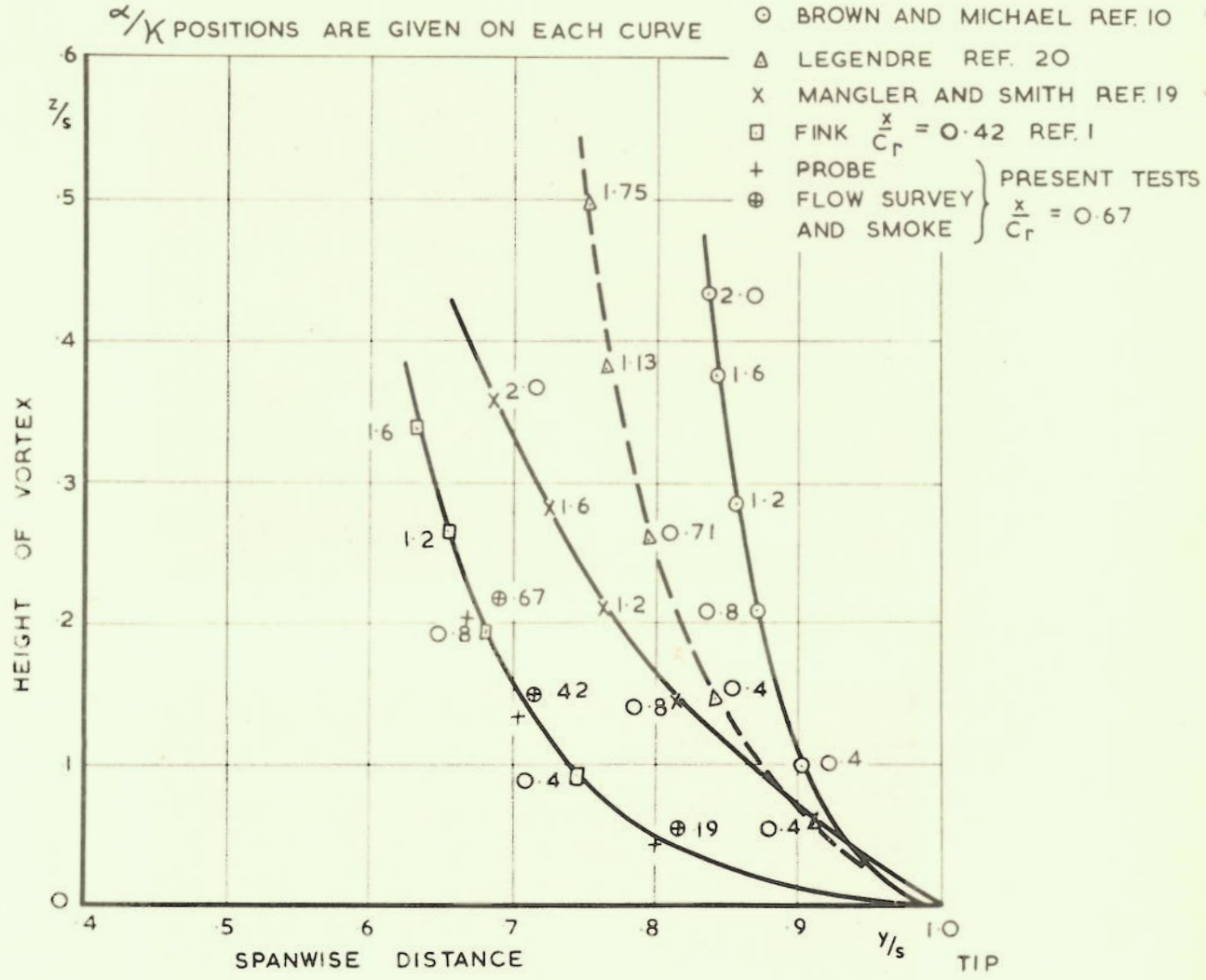

FIG. 19 VORTEX CORE POSITIONS

$\alpha = 14^{\circ}$

$\alpha = 29^{\circ}$

FIG. 20. SMOKE PHOTOGRAPHS AT STATION 2 ON 70° DELTA

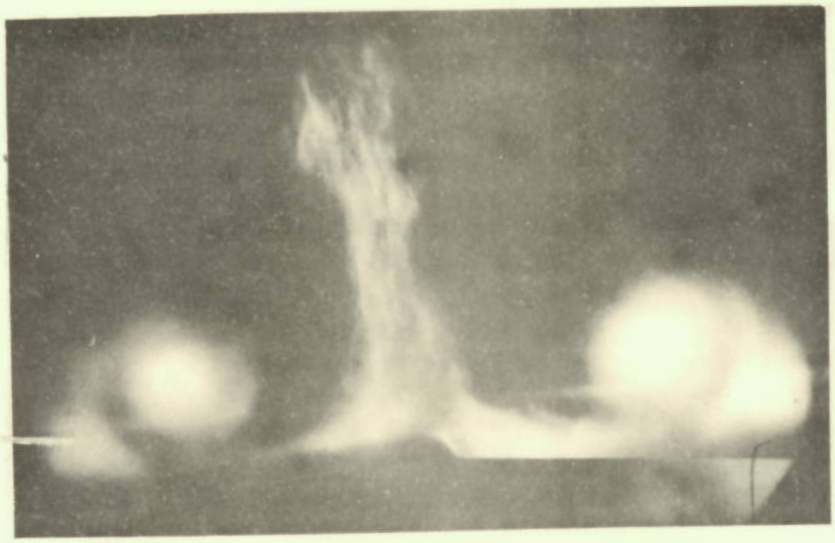

0.1 ROOT CHORD
BEHIND T. E.

0.2 ROOT CHORD
BEHIND T. E.

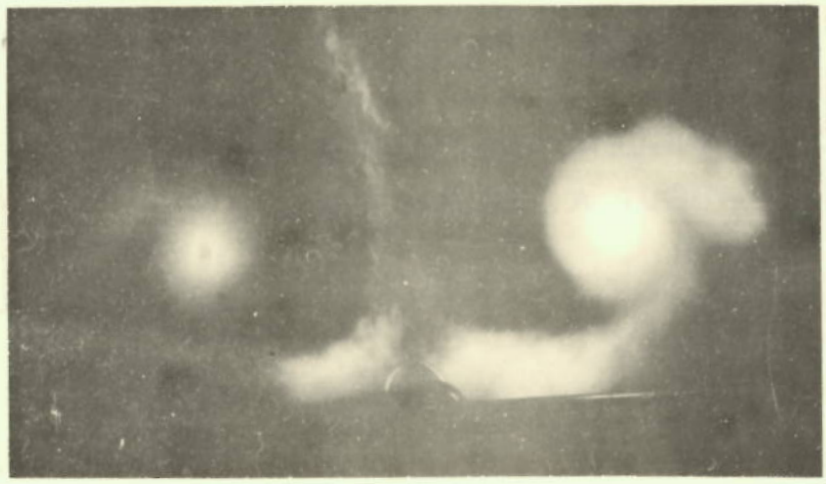

0.55 ROOT CHORD
BEHIND T. E.

FIG. 21. ROTATION OF SECONDARY VORTEX FLOW
AROUND MAIN VORTEX CORE AT α = 29

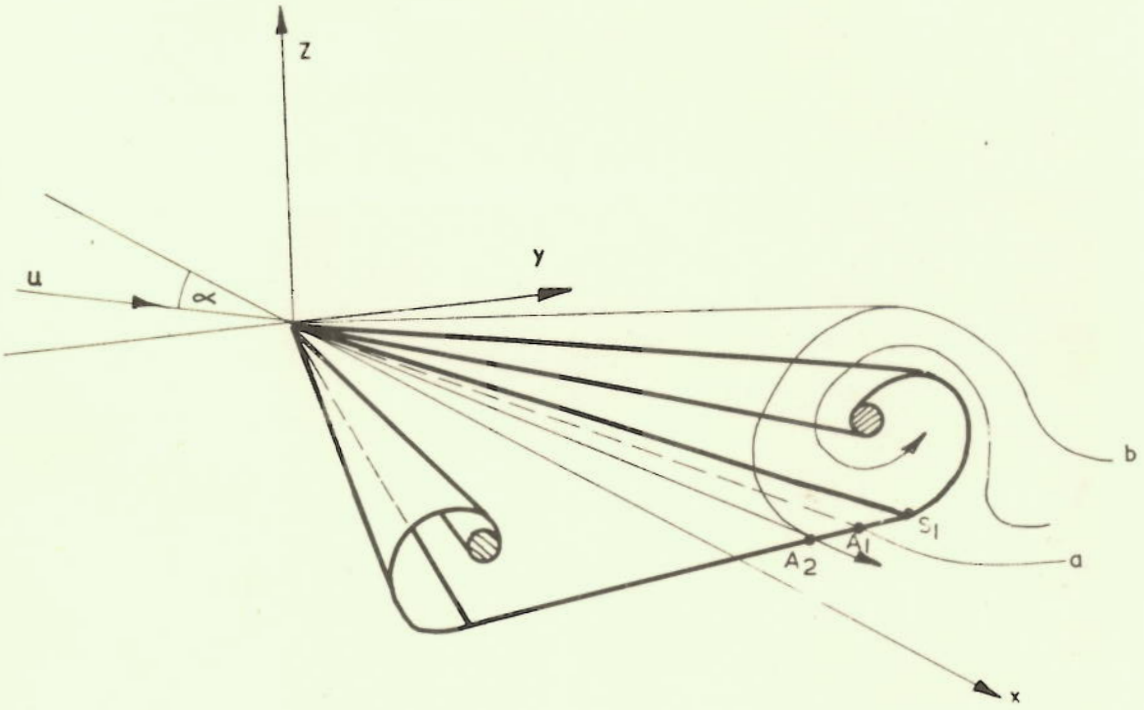

FIG. 22 SKETCH OF MANGLER AND SMITHS MODEL OF FLOW FIELD ABOUT A DELTA WING.

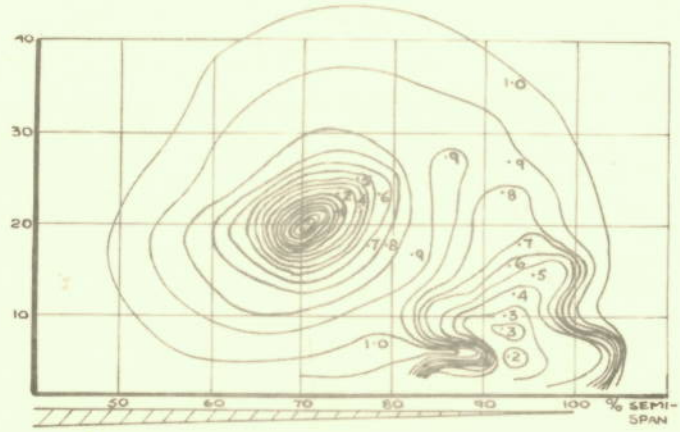

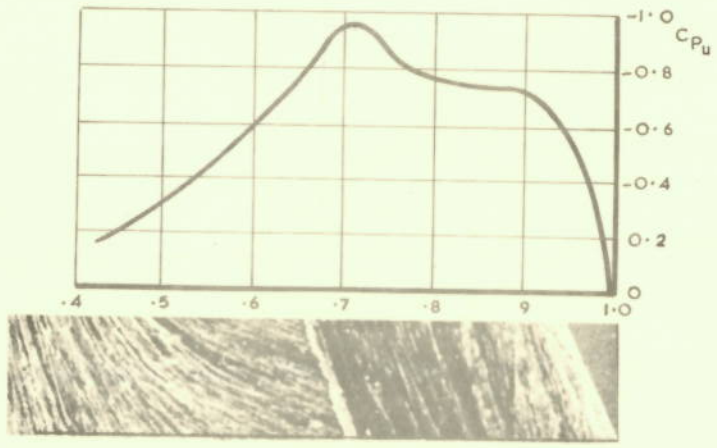

FIG. 23. COMPARISON BETWEEN FLOW VISUALISATION, TOTAL HEAD SURVEY & PRESSURE DISTRIBUTION AT STATION 2 $(0 \cdot 67 c_r)$
$\alpha = 14^\circ$ MODEL II $(\Lambda = 70^\circ)$

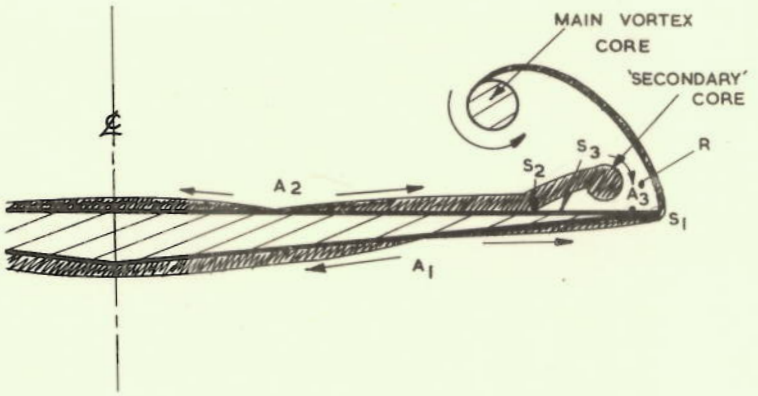

FIG. 24 THE VISCOUS REGIONS: $\frac{R}{K}$ =0·7
(BOUNDARY LAYER THICKNESSES EXAGGERATED.)

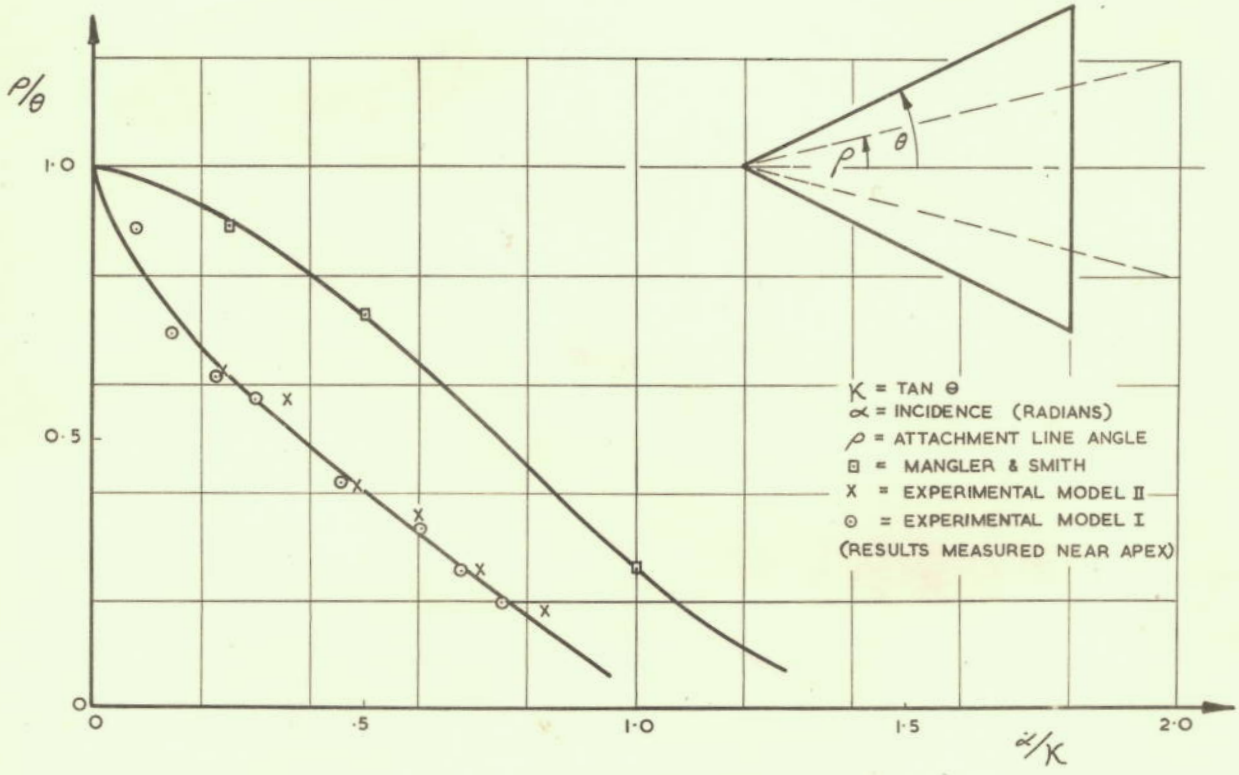

FIG. 25 SUCTION SURFACE ATTACHMENT LINE POSITIONS.

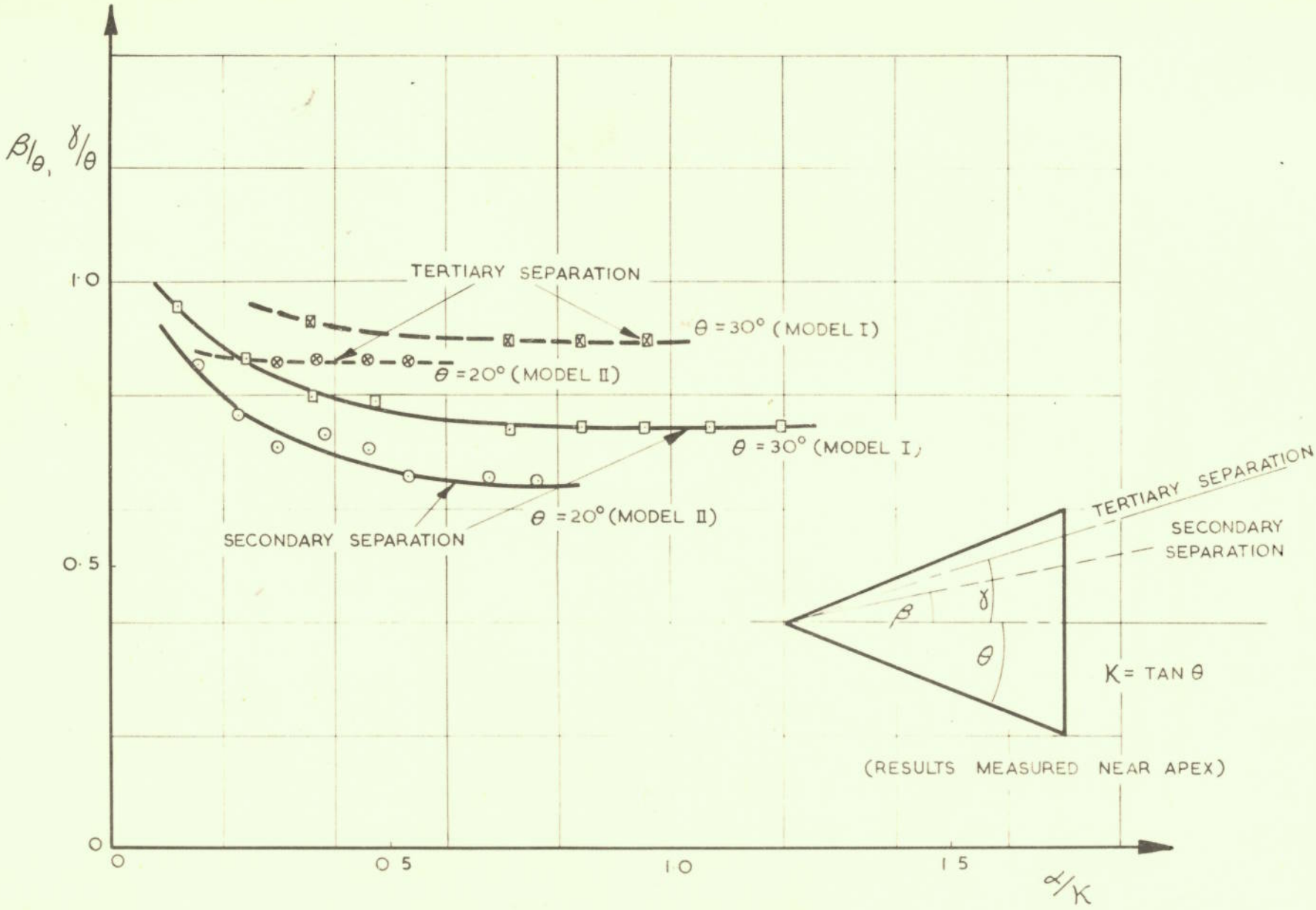

FIG. 26 SUCTION SURFACE SECONDARY AND TERTIARY SEPARATION LINE POSITIONS.